Pure Appl. Geophys. 168 (2011), 155–200

DOI 10.1007/s00024-010-0156-3

Pure and Applied Geophysics

Broadband Kinematic Stochastic Simulation of an Earthquake Source: a Refined Procedure for Application in Seismic Hazard Studies

Alexander A. Gusev[1,2]

Abstract—To carry out a realistic simulation of earthquake strong ground motion for applied studies, one needs an earthquake fault/source simulator that can integrate most relevant features of observed earthquake ruptures. A procedure of this kind is proposed that creates a broadband kinematic source model. At lower frequencies, the source is described as propagating slip pulse with locally variable velocity. The final slip is assumed to be a two-dimensional (2D) random function. At higher frequencies, radiation from the same running strip is assumed to be random and incoherent in space. The model is discretized in space as a grid of point subsources with certain time histories. At lower frequencies, a realistic shape of source spectrum is generated implicitly by simulated kinematics of slip pulse propagation. At higher frequencies, the original approach is used to generate signals with spectra that plausibly approximate the prescribed smooth far-field source spectrum. This spectrum is set on the basis of the assumedly known regional empirical spectral scaling law, and subsource moment rate time histories are conditioned so as to fit this expected spectrum. For the random function that describes final slip over the fault area, lognormal probability distribution of amplitudes is assumed, on the basis of exploratory analysis of inverted slip distributions. Similarly, random functions that describe local slip rate time histories are assumed to have lognormal distribution of envelope amplitudes. In this way one can effectively emulate expressed "asperities" of final slip and occasional occurrence of large spikes on near-source accelerograms. A special procedure is proposed to simulate the spatial coherence of high-frequency fault motion. This approach permits the simulation of fault motion plausibly at high spatial resolution, fulfilling the prerequisite for simulation of strong motion in the vicinity of a fault. A particular realization (sample) of a source created in a simulation run depends on several random seeds, and also on a considerable number of parameters. Their values can be selected so as to take into account expected source features; they can also be perturbed to examine the source-related component of uncertainty of strong motion. The proposed approach to earthquake source specification is well adapted to the study of deterministic seismic hazard: it may be used for simulation of individual scenario events, or suites of such events, as well as for analysis of uncertainty for expected ground motion parameters from a particular class of events. Examples are given of application of the proposed approach to strong motion simulations and related uncertainty estimation.

Key words: Strong motion, earthquake, simulation, scenario earthquake, uncertainty, stochastic fault model, coherence.

1. Introduction

In recent years, the amount of strong motion earthquake records has grown fast, and demands for more accurate estimates of future possible ground motions have simultaneously increased. These two factors define both the possibility of and the need for more efficient and reliable techniques to be used in creating such estimates. The field of deterministic seismic hazard is the main area of application of advanced methods of strong motion estimation. Specifically, in this field, determination of uncertainty for ground motion parameters is of primary importance, and any advanced methodology must be capable of such analysis. Usually, seismologically based simulation of earthquake ground motions includes description of: (1) earthquake source process, and (2) medium response caused by it. The second step may be rather complicated from the viewpoint of algorithm design for complicated media and also time consuming in practice, but it rarely presents conceptual difficulties. This is not so for the first step, which must include sufficiently realistic broadband specification of an earthquake source. In this case currently there is no commonly accepted approach; instead, there are several models and methods that are based, to a large degree, on hypothetic and/or oversimplified foundations. The

[1] Institute of Volcanology and Seismology, Russian Academy of Sciences, 9 Piip Blvd, Petropavlovsk-Kamchatsky 683006, Russia. E-mail: gusev@emsd.ru

[2] Kamchatka Branch, Geophysical Service, Russian Academy of Sciences, 9 Piip Blvd, Petropavlovsk-Kamchatsky 683006, Russia.

technique developed herein may represent a useful step ahead in this area. It should be emphasized that no new source model will be proposed: the aim of the study is to integrate the (mostly known) concepts in a way that permits efficient applied simulation for earthquake engineering applications.

To generate input for wave propagation calculation, one typically needs to describe evolution of finite fault/source in space and time. One should realize that, at present, there is a wide spectrum of such models: dynamical models aiming to clarify different aspects of fault evolution, models designed to fit observations of particular event(s), models intended for use in simulations of mostly high-frequency fault radiation (accelerograms), etc. In addition, for practical simulation of ground motion, there are semi-empirical or purely empirical models that partly or completely bypass fault slip description and aim at realistic description of empirical ground motion phenomenology.

There are two common approaches for describing earthquake fault evolution and related wave generation. The first approach, based on a solid tradition of long-period seismology, describes the fault process deterministically, in terms of fault slip rate as a function of time and position on a fault. The second approach, most useful at higher frequencies (HF), assumes that details of the propagating rupture are better treated in a stochastic manner. Most common techniques along these lines use fault models that consist of multiple subsources whose turn-on times are randomly or partly randomly phased.

Let us discuss in more detail the first (deterministic) approach, widely used both in fault simulations and in fault inversions. These inversions, first kinematic and later often dynamically constrained, provide our basic understanding of earthquake rupture process. Dynamic simulations and dynamically constrained inversions are based on the elastodynamic representation of a fault. While this approach is conceptually highly attractive and uses efficient numerical techniques, it meets certain obstacles. The first problem is that it is not easy to emulate an important property of fault motion, i.e., localization of slip process in a narrow running strip (Haskell, 1964, 1966; "slip pulse" of Heaton, 1990). However, some solutions to this problem have been proposed (e.g., Beroza and Mikumo, 1996; Ide and Takeo, 1997). A more important deficiency from the viewpoint of the present study is the inability of present dynamic models to efficiently predict the empirically known features of HF radiation. Of course, using a sufficiently detailed numerical grid and sufficiently expressed heterogeneous stress and/or strength field over a fault area, one can simulate a dynamic rupture with almost any level of HF radiation. The problem is how to perform this in a way that realistically emulates the HF properties of observed accelerograms. In particular, typically it is difficult to create high-frequency spectral shapes with flat source acceleration spectrum (like the common ω^{-2} spectral model). Second, dynamically based approach at high frequencies predicts enhanced forward directivity (Boatwright, 1982) that is seemingly too strong as compared with observations (Tsai, 1997a; Boatwright *et al.,* 2002).

Let us now discuss stochastic approaches. The first among these is the composite-subsource approach. Housner (1955) explained the noise-like and broadband character of accelerograms by a multitude of randomly fired dislocations with a broad spectrum of sizes. Since then, aggregates of dislocations/subearthquakes with broad spectrum of sizes, often with power-law ("Gutenberg–Richter-like") size distribution, were used as a model of a broadband source. Blandford (1975) and Hanks (1979) tried to explain in this way the power-law HF tail of the Aki-Brune (ω^{-2}, or more generally $\omega^{-\gamma}$) source spectrum; space–time structure of a source was not defined in these models. Following this line, Zeng *et al.* (1994) cover fault surface by several populations of circular cracks with hierarchy of sizes. This incoherent source model was systematically applied to produce realistic simulated strong motion. The similar model of Koyama (1985) was successful in explaining complicated, "humpy" shapes of source spectra of large-magnitude earthquakes. Note that these and many later models of this kind have no clear geomechanical foundation; rather, they represent some reasonable guesses put forward to explain empirical data. The main deficiency of such models is of tectonophysical nature: these "multiple-layer" composite-crack models with stress drop values comparable to that of the entire composite fault must

implicitly assume that rupturing at a certain fault point takes place several times during an earthquake; this seems to contradict to the results of inversions and direct observations of earthquake ruptures.

The first "single-layer" composite-crack model successfully tested against observations was the "specific barrier model" of Papageorgiou and Aki (1983, 1985). Similar-sized cracks of this model do not overlap, making this model tectonophysically permissible. A close concept was developed by Beresnev and Atkinson (1999). Less studied are "single-layer" composite-crack models with multiple-sized crack population (Irikura and Kamae, 1994). Despite certain achievements, models of this kind cannot be considered as tectonophysically plausible, for the following reason: Subcracks of these models, always with high stress drops, are separated by unbreakable barriers that do not fail during an earthquake, so that the geological dislocation does not span the entire fault surface in a continuous manner. This possibility is apparently supported by the observation that surface fault traces created by a particular single earthquake often show near-surface en echelon structure, so that the amplitudes of geologically observed slip seem to vanish at some points. However, when one considers long-term fault history, the idea of strong residual barriers becomes much more doubtful: tectonic evidence testifies that fault dislocation accumulates more or less steadily in geological time, through repeated hundreds and thousands of earthquakes with similar direction of slip. The only way to reconcile these facts is to assume that strong intersubcrack barriers yield and fail in aseismic manner between earthquakes. However, these barriers must be very strong (order of kilobar/100 MPa of static load, plus excess from dynamic loading), and their aseismic failure looks highly improbable. It should be noted that models of this kind may permit one to emulate broadband observations quite realistically (e.g., Hartzell *et al.,* 1999, 2005).

To overcome difficulties of composite-fault and dynamic-crack approaches, one might combine their strong sides: mechanically well-founded model, and the stochastic mode of HF energy generation. In particular, one may introduce nondeterministic properties of rupture front. Along these lines, a fault rupture propagation model with randomly fragmented front was proposed on the conceptual level (Gusev, 1989). It relates HF seismic signals not to subcracks but to subsources of another kind, namely small strong patches over the fault surface, or small asperities ("strength asperities") of the kind proposed by Das and Kostrov (1983). Subsources of this kind are tectonophysically highly plausible because the contact of rough fault walls must create just this kind of strength distribution. Recently asperities of this kind have been revealed in inversion (Dreger *et al.,* 2007). Gusev (1989) assumed that small (order of 1 km size) "strength" asperities cover 2–10% of the entire fault surface and that their probability distribution of strength is heavy-tailed. (This term is applied when relatively large values of random variate are much more common as compared with the standard case of the Gaussian distribution; in other words, the probability distribution has an enhanced tail; typical examples are the lognormal law and the power law, also called the hyperbolic and Pareto law.) The idea of a heavy-tailed strength distribution was originally derived from the fact that powerful spikes are often observed in accelerograms recorded in the vicinity of faults (i.e., the amplitude distribution of acceleration is non-Gaussian and heavy-tailed itself). The concept of multiple small asperities with heavy-tailed probability distribution of strength permitted consistent explanation of many properties of observed HF radiation. Although this approach was never developed into a practical simulator, the dynamical model of Das and Kostrov (1988) illustrates its possible behavior in the case when the number of "strength asperities" is small. Instructive in this respect is the model of Silberschmidt (2000), who traced quasistatic crack propagation through a randomly damaged elastic medium and has shown how a highly fragmented, tortuous rupture front may arise and propagate. As was formulated by Gusev (1989), during the formation of the crack/rupture, although 'its front propagates "macroscopically smoothly",…"microscopically" this rupture propagation is a wave of breaking of (small) asperities.' In other words, if viewed at low resolution, a fragmented rupture front may be hardly distinguishable from an ideal continuous brittle crack tip with a single well-defined singularity: both look similarly if

only long wavelengths are analyzed. One can believe that a fragmented, incoherently radiating rupture front is a characteristic feature of a real earthquake process on small space–time scales. The present paper is conceptually based on this viewpoint. Recently this view was strongly supported by a quite similar concept of DAY *et al.* (2008), who found that, to create deterioration of directivity at high frequencies, one should "model rupture complexity in a form that permits rupture to be omnidirectional at small length scales, even though unidirectional at large scales," whereas simple modulation of the magnitude of slip rate over a fault cannot effectively suppress enhanced forward directivity. Note that the assumption of a multitude of strong small asperities is simultaneously a simple way to explain large (non-Gaussian) acceleration spikes. The capability to reproduce occasional but systematic occurrence of such spikes is an important requirement for an efficient practical strong motion simulation methodology.

In another, conceptually more formal and systematic approach, instead of introducing a multitude of tectonophysically more of less plausible subsources, one treats slip rate in space–time as a random function. The first such description, by HASKELL (1966), was modified by AKI (1967) and represented a critical step in establishing the now standard ω^{-2} source spectrum model (BRUNE, 1970 presents its simplified deterministic variant). In both models, random broadband slip rate was assumed to be governed by its correlation function in space and time. In textbooks, correlation function is introduced for random stationary functions defined on unbounded domains. Both HASKELL (1966) and AKI (1967), however, apply the definition of correlation function to a process defined in a finite volume of space–time. This may do little harm when applied to frequencies much above corner frequency, but is disturbing when correlation time is of the order of signal duration. This problem was avoided by ANDREWS (1980, 1981), who makes no attempt to describe the entire source function as a random object, and separates it into two parts: (1) the deterministic part that defines source size and "corner period," with smooth behavior in space and time, and low amplitudes at HF; and (2) the stochastic HF and high-wavenumber (HK) part, assumed to be fractal, so that its average HF and HK power-spectral behavior follows the power law, and whose contribution around and below corner frequency and corner wavenumber is negligible. This stochastic part is constructed in two steps: first a sample random field is modeled over an unbounded space–time; then it is windowed, and the size of this window over time and space accurately matches the size and duration of the deterministic component. Despite the fact that Andrews' model ignores rupture propagation, his approach seems attractive, and represents another starting point for the technique developed below.

If one limits oneself to HF signal only, one can apply the asymptotic description of the wavefield (SPUDICH and FRAZER, 1984; BERNARD and MADARIAGA, 1984) that permits detailed description of the fault slip and rupture front propagation. In this manner, HERRERO and BERNARD (1994) combined random fractal field of slip, and simple deterministic kinematics of the rupture front to produce an effective representation of HF wavefield. It was soon tested against real data (ZOLLO *et al.,* 1997), with limited success. A significant advantage of the models based on random-function description of a fault is their potential for prediction of ground motion in the immediate vicinity of a fault. Indeed, observation-based random function description can be extrapolated to high frequencies and wavenumbers, at least in principle. No other approach shows good promise in this respect. Still, this rupture model seems to produce too high levels of HF amplitudes in the forward direction, probably because it includes randomization only in space.

One more stochastic approach, less general but important, is to treat an earthquake source at high frequencies by considering the space–time distribution of HF radiation power (more accurately, HF luminosity) over the space–time volume of a source. In this case, fault slip rate at high frequencies and high wavenumbers is again assumed to be a random function. Therefore, wave contributions from different fault patches combine with random phases, and the additivity is present for wave instant power (wave intensity, mean squared amplitude) and not for amplitude proper. The idea of incoherent earthquake source is after KOSTROV (1974), and its first detailed formulation is provided by GUSEV (1983). The source

description in terms of HF power can be conveniently performed separately for a set of frequency bands that jointly cover an entire HF part of the source spectrum; e.g., KOPNICHEV and SHPILKER (1978) successively emulated along these lines the then-famous near-fault accelerogram of the Gazli 1976 earthquake. Similar representation of a source was successfully applied to inversion of luminosity function (GUSEV and PAVLOV, 1991) and to the description of HF radiation field around a fault (GUSEV, 1983; TRIFUNAC and LEE, 1989; PAPAGEORGIOU and AKI, 1985; SINGH *et al*., 1989; OHNO *et al*., 1993). It also emerged to be highly efficient in providing theoretical background for interpretation of macroseismic data (GUSEV and SHUMILINA, 2000). It should be mentioned that also the effects of propagation of HF waves at local to regional distances can often be expressed as instant power time histories or envelopes, and both descriptions—of a source and of medium effect—can be directly combined merely by convolution of time functions of instant HF power. Convolution is usable because of the additivity of instant-power time functions for random signals (GUSEV, 1983; GUSEV and PAVLOV, 1991). Still, by this approach one cannot represent signals with wavelengths comparable to that of entire fault; thus it cannot provide broadband source description if used alone. Another weakness is that it is difficult to trace the evolution of probability distribution of a signal in the important case when it is non-Gaussian.

A less general, but widely and often successively employed approach, based on the point source representation of an incoherent source, uses BRUNE's (1970) ω^{-2} representation of source spectra. Essentially deterministic, analytical amplitude spectra of BRUNE (1970) are used in this case as if they represent root-mean-square (rms) amplitude spectra of random signals. This approach (HANKS and MCGUIRE, 1981; BOORE, 1983; see BOORE, 2003 for detailed review) is frequently referred to as "the" stochastic method. A comparable approach was developed by GUSEV (1983) on the basis of a more realistic semi-empirical spectral scaling law with no simple scaling. It had also some additional advantages: it included theoretically founded description of saturation of HF amplitudes in the vicinity of the finite fault and it accounted for effects of scattering on duration. The practical procedures for simulation of HF strong ground motion and its parameters on this basis are described in by PARVEZ *et al.* (2001) and PETUKHIN and GUSEV (2003).

One more simulation technology stands somewhat by itself: the methodology called "Recipe," which has recently been developed by Irikura and coworkers (IRIKURA, 2007). It was widely tested against observed data and also applied for deterministic seismic hazard mapping of Japan. The original algorithm included the following steps: (1) for a given position of a fault within the Earth, a compatible combination of fault area S, seismic moment M_0, and global stress drop $\Delta\sigma_{gl}$ is selected; (2) the probable number of simply shaped asperities (usually two to three), the nucleation point position, and the value of rupture velocity (for assumedly circular rupture) are chosen; (3) summary area of asperities S_a is derived on the basis of empirical study (SOMERVILLE *et al.*, 1999); (4) local stress drop $\Delta\sigma_a$ over asperity area is determined from S_a, S, and $\Delta\sigma_{gl}$; (5) effective stress on asperities σ_a is estimated as approximately equal to $\Delta\sigma_a$, and effective stress on background (nonasperity) part of the fault σ_b is determined from the balance, at given $\Delta\sigma_{gl}$ and $\Delta\sigma_a$, of global stress and local stress; (6) earthquake fault is represented by a grid of subsources whose local slip rate time history is constructed combining the smoothed $t^{-0.5}$-kind shape function and the absolute value derived from the values of local effective stress, rupture velocity, and f_{max} through the relationship derived from the results of dynamical simulation of a nonuniform crack. The model appears completely deterministic. After convolution of source representation with realistic, random looking medium response [represented by empirical Green functions (EGF)], accelerograms are generated that are random looking and emulate the observed ones rather well. In particular, forward-directivity pulses are effectively generated. The need for appropriate EGFs may complicate the use of this approach in areas of low to moderate seismicity. It also may be difficult to select positions and sizes of individual asperities over a surface of a scenario fault.

From this short review one can see that there is no completely consistent, tectonophysically founded, and numerically efficient approach that might

be taken as a basis for developing practical simulation procedure usable for deterministic hazard analysis. The particular scheme further described herein is an attempt to balance positive aspects of the presented approaches, keeping the algorithm both geophysically sound and matched to empirical evidence regarding strong motions. In addition to the general concept of simulation procedure, a workable algorithm must be accompanied by a set of relevant relationships, their functional forms and parameterizations, and also by a set of default values and reasonable brackets for the parameters employed. In general terms, one needs to specify a three-dimensional (3D) space–time ($X \times Y \times T$) random function of local slip rate. This problem will be decomposed into a number of subproblems that can be parameterized in a relatively independent manner. Of course, neither the decomposition nor the selection of the parameter set is unique; our particular choice was carefully planned and represents a significant element of the presented methodology. The following subproblems are most significant:

– Geometric and kinematic scaling of a fault, including global stress drop, Mach number, and aspect ratio;
– Specification of (random) rupture front history in space–time;
– Specification of 2D random function of final slip or of stress drop; in the selected parametrization, one must set the power spectrum of final slip, the probability distribution of values, and the window function that defines a finite fault;
– Specification of a set of one-dimensional (1D) local slip rate time histories for discrete subsources that represent the fault numerically; this again includes power spectrum, the probability distribution of values, and the window function (mostly defined by rise time).

The key element of the proposed approach is that the power spectrum of local slip rate time histories is not set explicitly; instead, it is defined implicitly from the condition that far-field amplitude spectrum of the simulated source agrees with the assumed source spectrum (defined, e.g., by the regionally specific scaling law).

To select particular versions of the listed relationships, the corresponding published evidence and theoretical concepts were reviewed and analyzed, and some particular choices were made; these are discussed in more detail later.

Below are listed the requirements that can be derived from the above discussion and that were taken as key ones for the design of an advanced earthquake fault simulation technique, addressed to practical applications:

- The technique should smoothly combine low-frequency and high-frequency descriptions of a fault, and incorporate into these descriptions most well-established properties of observed faults and strong motions;
- Low-frequency description must be based on the slip-pulse (running strip) rupture model and on a self-similar random structure for final slip;
- High-frequency description must reproduce source spectrum that can be assumed to follow our empirical knowledge of observed Fourier spectra at moderate to large distances;
- Probability distributions of simulated random functions describing slip in space and local slip rate in time must be selected so as to emulate observed properties of final slip distributions and of accelerograms; in particular, occasional powerful acceleration spikes must be present in simulated traces.

The approach presented below is aimed to satisfy these groups of requirements. The source, or in practical terms the set of time histories of subsources, is generated in two consecutive steps. At the first step a "preliminary" source is generated, with a realistic low-frequency behavior and a partly realistic HF behavior. The properties that are simulated appropriately are: rupture front history, rise time, final slip distribution (slip map); and, as regards time histories of subsources, the structure of envelope and the probability distribution of amplitudes (a heavy-tailed one). The only unrealistic feature of these time histories is their spectral behavior: the HF level of their amplitude spectra is too high. This deficiency is amended at the second step: preliminary time histories are smoothed in an accurately controllable manner, fitting an empirical spectral scaling law

(defined for the far field). During practical calculation of a scenario earthquake, common further steps follow: calculation of Green functions for subsource–receiver pairs and convolution over space–time volume of the source. These steps are not discussed here; a reader may refer to GUSEV and PAVLOV (2009) for more details.

In the following presentation of the developed methodology, I shall also refer to certain particular implementation details that seem to be relevant in a paper treating the matters of an applied simulation. Also, particular algorithms seem to be the best (and tested) practical illustrations of the general concept. Two versions of the developed code called PULSYN will be mentioned sometimes: PULSYN2003, the earlier version used in most example calculations, and the more advanced current version, PULSYN2008.

The bulk of the paper consists of the following parts: (1) an outline of the simulation procedure; (2) algorithms for the stages of source simulation, with parallel discussion of the input parameters, their determination, and assumed typical values; (3) a technique of uncertainty estimation; and (4) example strong motion simulation results, including in one case the example uncertainty analysis.

2. *Outline of the Simulation Technique for a Broadband Earthquake Source*

Within the present approach, an earthquake source is defined by dislocation time history $D(t, x, y)$ over a planar rectangular area in the (x, y) plane, with nonnegative slip rate $\dot{D}(t, x, y)$. Unit seismic moment tensor of the source, defined by slip direction and fault-normal direction, is assumed to be constant over the fault area and in time. Therefore, the description of the source in space–time is essentially scalar, in terms of the scalar seismic moment density, or, rather, its rate.

To specify temporal and spectral properties of simulated sources, I shall widely use the equivalent point source representations: corresponding moment rate time history $\dot{M}_0(t)$, its Fourier transform $\dot{M}_0(f)$, and its modulus or amplitude spectrum ("source spectrum") $\left|\dot{M}_0(f)\right|$. Constant factor aside, these functions coincide with time history and spectrum of body wave displacement as observed (in uniform unbounded medium) at a ray normal to the fault plane, and will also be referred to as "displacement" time history and spectrum. In a similar manner, I shall speak of "velocity" time history and spectrum ($\ddot{M}_0(t)$, $\ddot{M}_0(f)$, and $\left|\ddot{M}_0(f)\right|$), and "acceleration" time history and spectrum ($\dddot{M}_0(t)$, $\dddot{M}_0(f)$, and $\left|\dddot{M}_0(f)\right|$). Note that seismic moment $M_0 = M_0(t)|_{t=\infty} \left|\dot{M}_0(f)\right|\big|_{f=0}$.

The slip rate function is simulated using the generalized version of the classic HASKELL (1966) stochastic fault model. Following this model, local slip rate $\dot{D}(t|x, y)$ is assumed random and nonzero over a definite duration, denoted "rise time" T_{rise}, whose value is significantly smaller than the total rupture duration. Rupture propagates along the fault area, forming rupture front; its shape is circular or random-like, and its velocity is a random function of distance from the nucleation point, or of position on a fault. Similarly, final slip is a random function $D(t = \infty|x, y) \equiv D(x, y)$; it is specified through its power spectrum PSD(k); following ANDREWS (1980), it is described by a power law: PSD(k) $\propto |k|^{-2\gamma}$. The key idea of generating realistic broadband ground motion is to require that source spectrum $\left|\dot{M}_0(f)\right|$ in its high-frequency part can be derived on the basis of averaging of observations in the study region; it need not (though may) follow any theoretically preferred (e.g., Aki-Brune ω^{-2}) form. This smooth "target spectrum" serves as an input to simulation, and local slip rate time histories are adjusted so as to reproduce this spectrum in the rms sense.

To realize these ideas numerically a rectangular grid of point-like dislocation subsources representing equal-area cells is introduced, typically nearly square shaped. Thus, the general case of simulating entire 3D ($X \times Y \times T$) source function is reduced to generating a finite number of appropriate time functions of seismic moment rate for each subsource. Each of these time functions are generated by means of convolution of two components. The first component is called "preliminary subsource time history." It is a segment of nonnegative random noise, with amplitude spectrum that is slowly decreasing or flat ("pink" or "white"). Preliminary subsource functions are individual for each subsource, and constructed in such a manner that they bear many critical significant features of final time histories. Each such function has:

(1) correct timing of onset defined by simulated rupture front propagation, (2) desired duration and mean envelope shape, (3) desired probabilistic properties, i.e., the degree of non-Gaussian behavior or "spikiness," and (4) desired value of integral, equal to subsource seismic moment M_{0i} [defined in turn by the simulated $D(x, y)$ function]. As the general style of the space–time source behavior and its numerical parameters are chosen to be realistic, the "preliminary source," or the space–time object that consists of all preliminary time histories of subsources, reminds one of a real source in many respects. However, through the described simulation procedure one cannot directly construct waveforms with empirically plausible HF far-field spectral shapes. This goal is attained in two steps. First, the "preliminary source" is generated in such a manner that its HF spectral amplitudes are deliberately overestimated. To amend this deficiency, convolution is then performed with an accurately designed "finishing operator" which is essentially a smoothing operator.

Subsources of the present model serve only as a tool for numerical simulation of an incoherent source with mostly uncorrelated spots; they have no direct physical meaning. The number of subsources can be large. Each subsource bears a certain fraction of the total seismic moment of the source. The distribution of seismic moment over subsources is governed by the aforementioned random final slip function $D(x, y)$, simulated over the low-wavenumber spectrum range, from $k = 1/(\text{fault size})$ up to $k = 1/(\text{cell size})$. Seismic moment of a subsource is directly related to the integral of slip over its area. The duration of a subsource is defined by T_{rise}. In the earlier version of the procedure (PULSYN2003) the HF components of the moment rate time histories of subsources are generated as pairwise uncorrelated random functions; implicitly, this approach means that correlation lengths of planar HF radiator are similar for all frequencies and equal to intersubsource distance. However, following the general concept of Gusev (1983), correlation lengths must be frequency dependent. This property is incorporated into the recent PULSYN2008 version.

A simplified flowchart of the simulation procedure is shown in Fig. 1. For each step, a list of critical input parameters is shown on the left. A variant is given with a particular set of inputs when fault length L and width W are preset in combination with simulated event seismic moment M_0, so that the stress drop parameter is a dependent variable. Below are comments relating to the main simulation steps as indicated in the flowchart. Details of parameter lists will be clarified later.

1. Overall parameters. Key rupture parameters are specified here: average rupture velocity v_{rup0}, "unilateral rupture duration" $T_{\text{ul}} = L/v_{\text{rup0}}$, and stress drop parameter δ. At the same step, subsource grid, the size of time window, and time step are set.
2. Two-dimensional slip distribution. A random-field model of final slip is generated; it defines seismic moments of individual subsources M_{0i}.

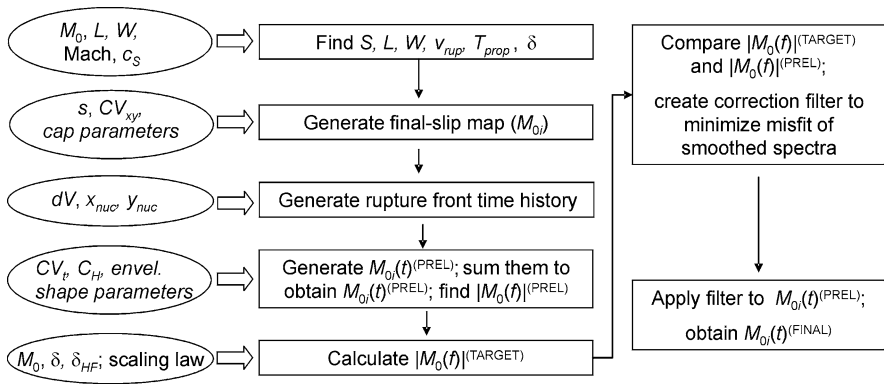

Figure 1
Flowchart of the source simulation procedure

3. Rupture front history. A predetermined nucleation point ("hypocenter") is set, permitting simulation of unilateral or other (symmetric bilateral, etc.) modes of rupture kinematics. Rupture front geometry is either axisymmetric, with circular front, or more general. In both cases, rupture velocity is a random function, either of distance from hypocenter or of position within the source rectangle. The arrival of the front at a point subsource turns it on.
4. "Preliminary" subsource time functions. For each subsource, random slip rate function $\dot{M}_{0i}^{(\mathrm{PRE})}(t)$ is generated, combining nearly white lognormally distributed stationary noise and envelope/modulation function whose general shape is predetermined and whose effective duration is defined by T_{rise}. The sum of all $\dot{M}_{0i}^{(\mathrm{PRE})}(t)$ delivers total source time function $\dot{M}_{0}^{(\mathrm{PRE})}(t)$; its Fourier amplitude spectrum $\left|\dot{M}_{0}^{(\mathrm{PRE})}(f)\right|$ is then calculated. In steps 2, 3 and 4, independent random seeds (or, in case of multiple runs, independent set of seeds) are used in generation of corresponding random functions.
5. Target Fourier spectrum $\dot{M}_{0}^{(\mathrm{TAR})}(f)$ (absolute value only). This is calculated on the basis of the preferred theoretical or empirical spectral scaling law assumed to reflect specific features (regional or other) of the source zone that generates the fault under simulation; the main parameters used here are M_0 and stress drop.
6. Correction operator. The ratio of $\left|\dot{M}_{0}^{(\mathrm{TAR})}(f)\right|$ to a smoothed version of $\left|\dot{M}_{0}^{(\mathrm{PRE})}(f)\right|$ is calculated, and the correction smoothing filter is constructed. In the time domain, correction filter has unit integral of pulse response and mostly positive coefficients.
7. Adjusting spectral shape by the use of the correction operator. Each $\dot{M}_{0i}^{(\mathrm{PRE})}(t)$ function is processed (smoothed) by the same correction operator of step 6, resulting in final subsource time function $\dot{M}_{0i}^{(\mathrm{FIN})}(t)$. The obtained set of functions represents the final source description that was sought; the sum of $\dot{M}_{0i}^{(\mathrm{FIN})}(t)$ exhibits an acceptable far-field spectrum.

Steps 6 and 7 are somewhat complicated technically because of the requirement that only the HF part of the preliminary spectrum must be smoothed, whereas its low-frequency (LF, low-resolution) part should be preserved.

Note that the directivity effects are well expressed in the radiation from the simulated source. To form directivity, appropriate set of delays of waves from different fault spots must be formed at the receiver. These delays are created automatically by the space–time structure of a finite rupture formed by means of multiple subsources and their accurate timing. In particular, the recently popular forward-directivity velocity pulses can be simulated with no explicit specification of these. However, it should be noted that, within the simulation procedure, it is assumed implicitly that the (empirical) target spectrum is associated with the signal radiated along the ray normal to the fault surface (so that signals from all subsources have no relative delays).

In a practical simulation of strong ground motion (for a rock site), next steps are calculation of Green's function (GF) for each subsource–site pair, convolution of $\dot{M}_{0i}^{(\mathrm{FIN})}(t)$ with corresponding GF, and summation over all subsources for a given site. These steps are outside the scope of this paper and are not discussed in any detail; they are necessary however for testing the procedure against observations.

3. *Stages of the Source Simulation Procedure, Relevant Methods, and Algorithms*

3.1. *Overall Fault Parameters*

In a source simulation procedure, a seemingly trivial but important step is to define an "overall" group of fault parameters—those that can be defined without specification of details of rupture process. We assume from the beginning that the simulated event is quantified by its seismic moment M_0 or equivalently by moment magnitude M_w. Two main variants are typical for the further reasoning. In the first variant, the general aim is the direct "forward" simulation of a scenario event. In the worst case one can know no more than the sole M_0 value; then all other fault parameters should be determined from default values of relevant coefficients or dimensionless parameters. Preferably, the value for a particular parameter should be selected on the basis of relevant information of

regional or local kind. Still, the set of default values for coefficients/parameters (or of typical bounds of their variation) is a significant component of the described practice-oriented approach.

In the second variant, the main aim of study is to test the simulation procedure through comparing its results with observed records. Then a large fraction of parameters is often known from the data analysis, and it is interesting to understand how many parameters among unknown ones must be significantly adjusted to provide acceptable match of simulated and observed signals.

In addition to M_0, the "overall" parameter group includes the length L and width W of the source rectangle, its area S, fault-average rupture velocity, and nucleation point position. Fault size, combined with M_0 value, define, to a large degree, the value of fault-averaged ("global"), stress drop value $\Delta\sigma_{\mathrm{gl}}$. It might seem conceptually attractive to introduce a reference, default value of $\Delta\sigma_{\mathrm{gl}}$. However, even in the case of constant stress drop over a fault, the accurate relationship between $\Delta\sigma_{\mathrm{gl}}$, L, W, and M_0 depends on dip angle, on depths of lower and especially upper edges of the fault surface; thus it must vary significantly from event to event (to be really accurate, one should also take into account the particular slip distribution over fault area, the vertical profile of elastic moduli, and finally accurate boundary conditions along fault edges).

To provide more convenience in the data adaptation aimed at a practical simulation, I apply a less strict approach based mostly on KANAMORI and ANDERSON (1975). First, note that

$$\log M_0 = 3/2\, M_w + \mathrm{const} = \log\mu + \log D + \log S = \log\mu + \log D/W + \log SW, \quad (1)$$

where S is the fault area and D is the average slip. Gross geometric properties of the earthquake fault are determined by the aspect ratio $\mathrm{AR} = L/W$ and by the global stress drop $\Delta\sigma_{\mathrm{gl}}$ that can be roughly approximated as $\Delta\sigma_{\mathrm{gl}} \approx \mu D/W$. However, as the source can be situated in various media, it is physically more adequate to use the strain drop $\Delta\varepsilon_{\mathrm{gl}} \approx D/W$. Dividing (1) by 1.5, and noting that $W = (S/\mathrm{AR})^{0.5}$, leads to (using new variables):

$$M_w = \log S + \left[2/3\ \log\ \mu + 2/3\ \log\ \Delta\varepsilon_{gl} - 1/3\ \log AR + \mathrm{const}\right]. \quad (2)$$

Denote by C_{MS} the value of the bracketed term. Often, a reliable empirical estimate of C_{MS} exists for a given event, equal to $M_w - \log S$. Also, for a region of study one can determine the average value of C_{MS} over many events, denoted by C_{MSref}. For a future event, one can substitute this value into (2) and try to estimate S from M_w, assuming "average" conditions, that is, for the case of the "average" stress or strain drop. As a default value of C_{MSref} one can assume, e.g., $C_{\mathrm{MSref}} = 4.1$ (SATO, 1979); this value agrees with predictions based on the average trends of WELLS and COPPERSMITH (1994). There is a scatter of individual-event C_{MS} values from the average; in addition, clear systematic trends occur.

A well-known phenomenon is the dependence of $\Delta\varepsilon_{\mathrm{gl}}$ and thus of C_{MS} on the return period of earthquake at the same position along a geological fault (KANAMORI and ALLEN, 1986); another, though correlated, factor is the intraplate/interplate rupture position (SCHOLZ *et al.*, 1986). The effect of fault depth and of buried/surface-rupturing source is also significant. To incorporate such factors into the analysis, I introduce a new, "logarithmic global stress drop anomaly" parameter, denoted by δ, with default value of zero. This parameter reflects the deviation of $\log\Delta\sigma_{\mathrm{gl}}$ from its standard reference (e.g., regional average) value. For a particular event it is defined as $\log(\Delta\sigma_{\mathrm{gl}}/\Delta\sigma_{\mathrm{gl,ref}})$, but in practice can be estimated approximately as $\delta = 1.5(C_{\mathrm{MS}} - C_{\mathrm{MSref}}) = 1.5(M_w - \log\ LW - C_{\mathrm{MSref}})$. The δ parameter in our simulation procedure is a key tool for defining fault geometry in the case of unknown fault size. Note that, in a practical situation, the roles of C_{MSref} and of δ are complementary, and their use depends on the decision regarding what is taken as a regular case and what is considered as an anomaly. The δ parameter is also needed for tuning of source spectra. It is assumed that, when $\delta = 0$, one can use in simulations the standard average regional empirical source spectrum for a given M_w. With nonzero δ, one has to modify the spectral shape, adjusting correspondingly the value of corner frequency but preserving M_w.

When the (M_w, δ) pair is defined, one can determine rectangle area S through

$$\log S = M_w - C_{\mathrm{MSref}} - 2/3\ \delta; \quad (3)$$

furthermore, from S and AR (assumedly known), L and W can be found. To this end, the value of the

parameter AR must be set. For a practical procedure, it was found useful to introduce an average AR(M_w) relationship into our procedure (in addition to the option of user-defined value). For subduction earthquakes, the default relationship interpolates from AR = 1.5 at $M_w = 5$ to AR = 3 at $M_w = 8$. In a study of an individual earthquake, another case is more typical, when the combination (M_w, L, W) is known, and δ is a dependent parameter [equal to $1.5(M_w - \log S - C_{\mathrm{MSref}})$ from (3)]. In any case, at given M_w, some mutually compatible combination of source size and (approximate) stress drop shall be automatically selected.

For magnitudes above 7.5, the scaling of the kind (1, 2, 3) remains mostly valid for subduction earthquakes but is violated for crustal earthquakes, especially for long strike-slip events. One may try to rely upon (HANKS and BAKUN, 2002) for the latter case [note that AR(M_w) trends are also nonidentical for these data groups]. The break of the M_w versus S scaling (1) for crustal earthquakes should be considered as an empirical fact that is immediately related to the important controversy regarding so-called L-scaling and W-scaling models of fault scaling (SCHOLZ, 1982 and later discussion).

An important step is the determination of rupture duration and corner frequency. Strictly speaking, these parameters become known only after the simulation of rupture propagation history, performed at later steps of the procedure. However, one needs at least a preliminary estimate of duration, in order to select the time window duration for simulation that must bracket the expected signal duration. To this end, a preliminary duration T_{ul} is estimated, assuming unilateral propagation along length, with velocity $v_{\mathrm{rup0}} = 0.5c_S$; where c_S is average S-wave velocity around the simulated fault, and 0.5 is a guess for low Mach value. Therefore, $T_{\mathrm{ul}} = L/v_{\mathrm{rup0}}$.

3.2. *Stress Drop Specification: Definitions and Possible Complications*

The specification of stress drop (or δ) value for a particular practical simulation is complicated and needs wider discussion. In the previous section the global stress drop $\Delta\sigma_{\mathrm{gl}}$ was mentioned. Assuming that the depth of the center of the rectangle H_c, dip, L, and W are all fixed, one can believe that the δ parameter is directly related to $\Delta\sigma_{\mathrm{gl}}$. However this does not mean that practical procedures used for stress drop parameter estimation will reproduce this $\Delta\sigma_{\mathrm{gl}}$ value, at least on the average. Most accurate estimates of $\Delta\sigma_{\mathrm{gl}}$ are those that use low- (or zero)-frequency M_0 estimates, based on long-period surface waves and/or geodesy, combined with independent information on fault geometry; denote this case $\Delta\sigma$(LF); of comparable accuracy may be estimates based on inversion of fault kinematics. In other cases, source size is determined indirectly from spectra of observed body or surface waves that probe the vicinity of the corner frequency f_c of the event. In this way, estimates of corner frequency proper, and therefore of source characteristic time ("corner period" $T_c = 1/f_c$, an estimate of duration) can be derived. The estimates of source size ($2R$ or L) are deduced from T_c, making some conjectures regarding rupture velocity and unilateral/bilateral rupture propagation mode. Estimates of $\Delta\sigma$ obtained from M_0 and f_c in this way are less accurate, and denoted here as $\Delta\sigma(\mathrm{LF}, f_c)$.

However in a number of cases the spectral behavior around f_c is not directly analyzed, and the estimated value of f_c, is deduced by extrapolation of body wave spectral level from the 0.5–5 Hz frequency range to lower frequencies. This approach is based on faith in the standard single-corner ω^{-2} spectral shape after BRUNE (1970). Unfortunately, for large earthquakes this assumption very often represents an oversimplification. It is sufficient to note that THATCHER and HANKS (1973), trying to match observed spectra by the $\omega^{-\beta}$ spectral shape, systematically obtained β values around 1, and that GUSEV (1983), ATKINSON (1993), and ORDAZ and SINGH (1992) found that spectral shapes of moderate to large earthquakes clearly deviate from the single-corner shape, rather showing two corners or humps. It also worth mentioning that the original variant of the BRUNE (1970) ω^{-2} spectral shape has two parameters: f_c and ε; in the less popular case when $\varepsilon \neq 0$, this model features the intermediate ω^{-1} spectral branch and the second (upper) spectral corner. In the scope of this much more adequate spectral pattern, only the

frequency of the lower corner is related to the source size, whereas the upper corner (of disputable origin) defines the level of acceleration spectrum. However, a many estimates of f_c and $\Delta\sigma$ have been published based on observed HF spectral levels interpreted in terms of the oversimplified, single-corner ω^{-2} model. These estimates should be treated as valuable sources of information regarding typical source acceleration ($|\ddot{M}_0(f)|$) spectral levels, but they are mostly misleading as regards true stress drop or true corner frequency. One can denote such estimates as $\Delta\sigma$(HF).

Unfortunately, there is one more source of confusion in this field. Brune (1970) and many followers of his spectral approach calculated their results using formulas for a uniform half-space. In reality, even for a rock site, a correction for the response of layered medium must be introduced. For moderate to large earthquakes this correction may be ignored around f_c, but must be taken into account for HF spectral levels (Gusev, 1983). As a result, some researchers take layering into account when constructing $\Delta\sigma$(HF) estimates [denote such estimates as $\Delta\sigma$(HF1)], whereas others use a half-space medium model [denote such estimates as $\Delta\sigma$(HF2)]. These symbols are mnemonic because, from the acceleration spectral data, one typically obtains $\Delta\sigma$(HF2) close to twice $\Delta\sigma$(HF1). As a result, it is not unusual to meet for the same event $\Delta\sigma$(LF) = 12 bar, based on 100-s M_0 value and independent size estimate, $\Delta\sigma$(LF, f_c) = 25 bar (based on a spectral feature of body wave spectrum, related to the largest asperity, and another, smaller M_0 value associated with this feature); and a pair $\Delta\sigma$(HF1) = 50 bar and $\Delta\sigma$(HF2) = 100 bar both based on 0.5–5 Hz acceleration levels. It should be emphasized that this entire set of estimates contains no real contradiction, but of course is quite confusing. The significant mismatch between estimates of type $\Delta\sigma$(LF) and $\Delta\sigma$(HF) is very typical, and there is a tendency to call $\Delta\sigma$(HF) by a neutral term "stress parameter" instead of "stress drop" (to simplify matters, one more problem was ignored: the followers of so-called L- and W-models of slip-moment scaling must use different boundary conditions for stress drop determination from slip data and thus would derive significantly different estimates of global stress drop even from the same, accurately known slip distribution). The moral of this story is that one should be extremely cautious when trying to compile empirical data on $\Delta\sigma$ and related parameters in order to create a basis for scenario event characterization. Nonhomogeneous stress drop data should never be pooled, and, typically, nontrivial adjustments will be need if methodically dissimilar $\Delta\sigma$ estimates must be generalized.

One should also be prepared for the fact that natural earthquake populations need not follow the simple and often reasonable idea of magnitude-independent (or weakly dependent) $\Delta\sigma$(LF) or $\Delta\sigma$(HF). Singh *et al.* (1989) found that the observed trend of near-source peak accelerations of Mexican earthquakes contradicts to one expected assuming magnitude-independent $\Delta\sigma$(HF); in this case $\Delta\sigma$(HF) seems to decrease with increasing M_w. Similar, very clear trends were found by Halldorsson and Papageorgiou (2005) for two out of three large strong motion data sets. Opposite tendency was revealed by Gusev *et al.* (2002) for Vrancea earthquakes; in this case, $\Delta\sigma$(LF, f_c) looked stable in the M_w range of 4.5−6.5, but increased about three times in jump-like manner as M_w became larger.

From the above discussion it is clear that it is useful to have at least two characteristics of earthquake source spectrum at given M_0: one related to corner period/rupture duration, and another related to source acceleration spectrum level. The $\Delta\sigma$(LF) parameter serves well as the former characteristic; as another parameter one may select $\Delta\sigma$(HF) (or another related parameter). The difference between these characteristics, according to Izutani (1984), reflects the difference between average stress drop and its rms variation, both calculated over a fault area. An attractive alternative to use of the $\Delta\sigma$(HF) parameter is direct use of the HF level of source acceleration spectrum. Very instructive compilation of this parameter denoted as $A_0 = |\ddot{M}_0(f)|_{f\approx 0.5-5\,\mathrm{Hz}}$ can be found in Fig. 5 of Irikura (2007) based to large degree on Dan *et al.* (2001); see also work by Atkinson (1993) and Aguirre and Irikura (2007).

A significant factor that affects A_0 is related to the difference between buried and surface-rupturing faults (Dalguer *et al.*, 2008). Other things being equal, the latter, because of free boundary condition along the upper edge of the fault area, must and do

have lower values of $\Delta\sigma$(LF) and/or C_{MSref}, and thus A_0, as compared with buried faults. However, this transparent cause of inequality of A_0 values may be insufficient to explain observed degree of actual differences.

In an applied study when the information about features of particular source zones can be very limited, a valuable source of information regarding $\Delta\sigma$(HF) is the difference between true magnitudes M (where M is M_w or some older type) and their estimates $M^{(\mathrm{MACRO})}$ based on macroseismic data, or "macroseismic magnitudes" (Kawasumi, 1951; Rautian *et al.*, 1989; Gusev and Shumilina, 2000); for instance, if a definitely positive difference ($M^{\mathrm{MACRO}} - M$) is found for a subset of data from a certain source zone, this may be a good predictor of unusually high A_0 values for future earthquakes there. Other macroseismic parameters, e.g., felt area (Atkinson, 1993), can also be employed.

All this means that, in a practical simulation, one needs to control at least two stress drop parameters: $\Delta\sigma$(LF) and $\Delta\sigma$(HF) (or, equivalently, A_0). In the described simulation procedure, $\Delta\sigma$(LF) value is controlled through δ, whereas for $\Delta\sigma$(HF), two options are provided. In the earlier version (the PULSYN2003 code), A_0 is defined (at given M_w) using the sum of δ value and another similar tuning parameter δ_{HF} (called "HF log-stress-drop anomaly"), so that the correction term for log f_c equals $1/3(\delta + \delta_{\mathrm{HF}})$. This approach, with combination of two corrections, may be awkward; thus an additional option was included in PULSYN2008 code that permits direct use of the A_0 parameter as input. This is done of the basis of the two-corner ("2-Brune") spectral shape of Atkinson (1993), i.e., the sum of two humps, each of standard ω^{-2} shape. After slight modification of Atkinson's formula, the A_0 parameter can be directly included in the set of four parameters that specify the 2-Brune spectral shape. This approach shall be illustrated for the case of the 1971 Kamchatka event below.

In the entire presentation above it was implicitly assumed that the contributions to the radiated energy spectrum produced by various sections of the fault can be treated as similar in terms of their spectral shape. In other words, the larger the seismic moment of a particular fault section, the larger its contribution to the total HF energy (of a particular frequency band). Such an implicit assumption is common for all broadband composite fault models (composite-crack, multi-asperity). However, a few recent studies based on regional (Kakehi and Irikura1996; Nishimura *et al.*, 1996; see Nakahara, 2009 for review) and teleseismic (Gusev, 2006) data suggest that the degree of correlation between spatial distributions of slip and of HF radiation capability (radiant flux) is, typically, limited. Nakahara (2009) notes that, in most cases, HF energy is preferably radiated from the periphery of slip asperities and not associated with their maxima. This view seems to contradict the results of a series of Japanese studies (Kamae and Irikura, 1998; Miyake *et al.*, 2003; Morikawa and Sasatani, 2004; and later work), which found that the approach described as the Recipe in the "Introduction" permits successful broadband simulation of both LF and HF strong motion on the assumption that all radiation is mostly generated by 1–3 slip asperities. This discrepancy may be only apparent; it seems to be caused by the fact that simulated "flat-top" asperities of the "Recipe," with constant final slip, radiate no HF energy by their central parts, and all HF energy is radiated by their periphery (this is a general property of any constant-slip, constant-velocity fault model). With some complications of the procedure, it is generally feasible to incorporate the discussed fault property into simulation, e.g., by treating such fault parameters as $\Delta\sigma$(HF) or A_0 as position dependent. Still, such a fine degree of fault specification was considered premature.

3.3. *Subsource Size, Rise Time, and Subsource Pulse Duration*

Each simulated point subsource represents a particular cell, finite virtual subsource, of approximately square shape. Such subsources form a grid that tiles a rectangle of size $L \times W$. Denote as x and y coordinate axes along L and W, respectively, as n_x and n_y the numbers of subsources along x and y, and as $d_x = L/n_x$ and $d_y = W/n_y$ ($\approx d_x$) corresponding subsource dimensions. Denote as $d_{\mathrm{sub}} = (d_x d_y)^{0.5}$ the characteristic distance between subsources. Generally, one might hope to reduce, to some negligible level, biases caused by using discrete grid

representation by employing dense subsource grids. However, such grids may require a prohibitive amount of Green's function calculation, so usually some trade-off is needed. The minimum number of subsources that is required to represent the entire source adequately depends on the following factors:

1. The duration of average local slip time function or of its main peak
2. The distance $r_{\min}$ from the receiver/site to the nearest point of the source/fault
3. The required accuracy of reproducing source-generated signal.

The first factor is related to the need to represent the space–time structure of the source with no strong distortion. Pulses from individual subsources should smoothly overlap. This means that d_{sub} must be sufficiently small, i.e., smaller or, marginally, equal to the width of the running strip. Otherwise a simulated record will consist of individual isolated pulses created by widely separated point subsources, instead of a realistic, more or less continuously looking process.

There is certain interplay between the second and third factors. At large or moderate $r_{\min}$ (about W or larger), the main effect of the source space–time structure on variations of the recorded signal for various rays is the common directivity effect. It is well known that it is difficult to estimate rise time from records observed at such or larger distances; reversing the logic of this statement, one can expect that neither particular selection of rise time/running strip width, nor moreover the selection of a particular functional form for local slip rate time history, has significant effect on the signal for the case in question. The only requirement is that rise time is significantly smaller than propagation time. Thus, at such distances, one can ignore the fine details of the local slip rate and assume artificial, marginally large, rise time values; correspondingly, the required number of subsources used in a practical simulation may be relatively small (grids such as 13×5 may be sufficient).

At shorter source-to-receiver distances, more accurate approach is needed, and stricter requirements regarding d_{sub} appear. They follow from the simple consideration that it is highly undesirable that contribution from a single subsource would be dominating at the receiver. To prevent such a situation, d_{sub} must be selected sufficiently small, not larger than $(0.2–0.4)r_{\min}$.

Abstractly speaking, there is one more factor that might complicate the selection of d_{sub}: the need to reproduce the spatial structure of the fault slip rate accurately. Indeed, d_{sub} must be smaller than the size of relevant spatial details of $D(x, y)$. Within the present approach, this problem is nonexistent, because the (artificial) discrete representation of $D(x, y)$ is generated in the wavenumber domain with just the right degree of resolution, with neither excessive details nor excessive smoothing.

The practical implementation of the described logic is as follows. First, the value of rise time for a Haskell–Heaton rupture is calculated as

$$T_{\text{rise}} = C_H L / v_{\text{rup0}} = w / v_{\text{rup0}}, \qquad (4)$$

where C_H is a preset constant, denoted as such to remind of Haskell and Heaton. C_H is the ratio of the rise time to the (unilateral) rupture propagation time $T_{\text{ul}} = L/v_{\text{rup0}}$, and $w = C_H L$ is the characteristic width of the instant slipping strip on the fault. The numerical value of C_H can be assumed on the basis of estimates of HEATON (1990) and MIYAKE *et al.* (2003) to be around 10–15% of the total rupture duration. Then the usual "rise time" parameter (4) must be related to some particular parameter of the local slip time history. There is no common relationship of such kind. In the following I assume that the rise time parameter (T_{rise}) is equal to twice the first power moment value (that is, onset-to-centroid delay) for corresponding time history. This definition is compatible with HASKELL's (1964, 1966) original one, introduced for the case of boxcar envelope of slip rate time history. Note that in the current version of the procedure the value of rise time is assumed identical over the entire fault plane.

The time delay between far-field pulses from two adjacent subsources T_{del} is a complete analog of the time between arrival of "starting" and "stopping phases" from two sides of a square-shaped (sub)-source. Let v_{rup} be the value of local propagation velocity. T_{del} depends on the angle between the ray direction and the direction of local propagation velocity; in the worst case of 180°:

$$T_{\mathrm{del}} = d_{\mathrm{sub}}(1/v_{\mathrm{rup}} + 1/c_S^-). \quad (5)$$

It is easy to see that, to allow the pulses to overlap smoothly at the receiver, the value of T_{del} must be not greater than the half-width $T_{1/2}$ of the local slip rate pulse, or of its prominent peak if this exists. This idea is illustrated by a sketch in Fig. 2. In cases when assumed time functions are of simple symmetric shape, such as boxcar, triangle or parabolic segment, one can assume that $T_{1/2} = T_{\mathrm{rise}}/2$. Otherwise, one should equate $2T_{1/2}$ to the width of the mentioned peak, denoted T_{peak}. Limiting further derivation by the case of a simple symmetric pulse, one obtains the following condition on d_{sub}:

$$d_{\mathrm{sub}} \le T_{1/2}\left(\left(1/v_{\mathrm{rup}}\right) + \left(1/c_S^-\right)\right)^{-1}. \quad (6)$$

In the case when rupture velocity varies moderately, one might try to substitute v_{rup} in (6) by its average value v_{rup0}. Taken directly, this idea however seems to be misleading. Indeed, temporal slowdowns and even arrests are typical features of real ruptures and must be permitted in simulation. In such cases, v_{rup} becomes small, and this dictates, through (6), that d_{sub} should also be set small, requiring a prohibitively large number of subsources. This contradiction is, however, only apparent: it results from our intention to guarantee smooth envelope of summary far-field signal. To require this for a rupture with arrests is to require too much. Therefore, it is sufficient to insert in (6) some moderately low bound for local rupture velocity, such as (0.3–0.5) v_{rup0}, and to permit parts of the fault that rupture at lower velocities to create discontinuities in the far-field envelope.

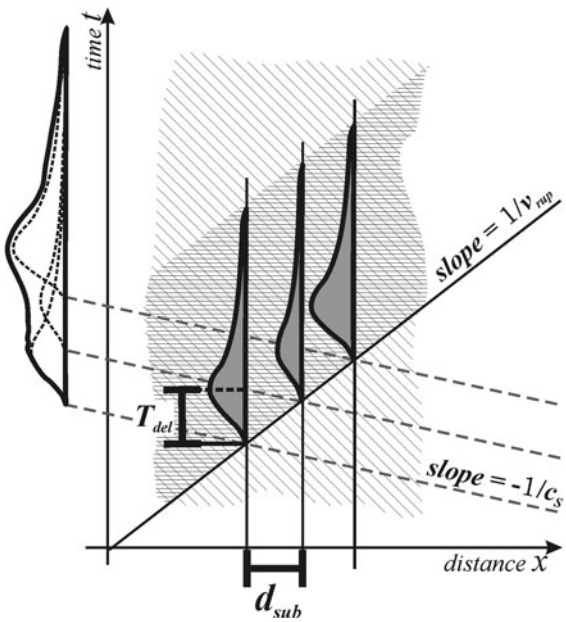

Figure 2
A sketch showing how to select intersubsource distance d_{sub} (identical to subsource size) for a grid of subsources whose envelope time functions have a certain characteristic time T_{del} (defined as the half-width $T_{1/2}$ of their main peak). Hatched area is a part of the x–t space–time plane, with the rupture front seen as a *solid line* of slope $1/v_{\mathrm{rup}}$. Space–time subarea that is slipping (with nonzero slip rate) is double hatched, and *grey shapes* represent local slip/moment rate time histories. On the *left*, far-field displacement pulse is shown for the "*backward*" ($-x$) direction of ray propagation; this pulse is formed by summation of contributions of subsources

After the recommended d_{sub} value is determined through (6), actual final values for d_x and d_y that are close to d_{sub} must be selected so as to make integer the numbers n_x and n_y of grid elements along L and W. In the "economy" case, when only the directivity effects are of interest, this same inequality (6) gives us a minimum artificial T_{rise} to fit given d_{sub}. In this case, only simple symmetric pulse shapes should be used.

It should be noted that, even in the case of delta-like local time history, far-field signals from a subsource of finite spatial dimension d_{sub} will be broadened with respect to such signals from a point subsource. To determine this broadening for the worst case one should solve (6) fixing d_{sub} and taking $T_{1/2}$ as the unknown. The average broadening for various rays and v_{rup} values is about $T_b = d_{\mathrm{sub}}/c_S^-$. Therefore, to account approximately for subsource finiteness, one may artificially increase the initial T_{rise} value from (4) to $T_{\mathrm{rise1}} = T_{\mathrm{rise}} + T_b$ [or better $= (T_{\mathrm{rise}}^2 + T_b^2)^{0.5}$].

In the case of small r_{min}, the described way to choose subsource size may result in unacceptably large values for d_{sub}. As noted above, a reasonable requirement for such a case is not to use d_{sub} values larger than $(0.2–0.4)r_{\mathrm{min}}$.

3.4. Setting Final Cumulative Slip Map, or Seismic Moments of Individual Subsources

An individual subsource time history (say, number i) represents the radiation related to fault motion over

its area Σ_i, with size of approximately $d_{\text{sub}} \times d_{\text{sub}}$. In theory, one operates with time history of local slip rate $\dot{D}(t,x,y)$. However, in implementation one has to discretize the fault. For waves with wavelength $\lambda \geq d_{\text{sub}}$, one can work with average slip rate over subsource area $\overline{\dot{D}(t,x,y)}$, directly related to the time history of subsource seismic moment rate:

$$\dot{M}_{0i}(t) = \mu \Sigma_i \overline{\dot{D}(t,x,y)} = \mu \int_{\Sigma i} \dot{D}(t,x,y) d\Sigma. \quad (7)$$

In its lowermost-frequency part in particular, this motion is characterized by its integral, or the (final, cumulative) seismic moment of subsource.

$$M_{0i} = \int \dot{M}_{0i}(t) \mathrm{d}t. \quad (8)$$

However, for waves with short wavelength $\lambda < d_{\text{sub}}$, (7) becomes invalid. The essence of the presented approach to simulation is that usable broadband $\dot{M}_{0i}(t)$ function, which includes in particular frequencies where (7) becomes invalid, is generated in an indirect way, to be discussed later in detail. Here we consider the limited problem of how to simulate the set of M_{0i} values in a realistic way. Following the tradition described above, it is assumed that: (1) the final fault slip can be represented by a realization (sample function) of a 2D random process over the rectangle, with a certain power spectrum; and, moreover, that (2) the shape of this power spectrum follows a power law (is hyperbolic), so that 2D power spectrum density (PSD) is:

$$S'\left(k_x, k_y\right) = S(k) = \text{const} \cdot k^{-2\gamma}. \quad (9)$$

Wavenumber vector is $k = (k_x, k_y)$; $|k|^2 \equiv k^2 = k_x^2 + k_y^2$. This PSD is isotropic in the (k_x, k_y) plane. The value of the exponent γ (slope of amplitude spectrum) is an input parameter of simulation.

This approach to simulation of fault slip is based on a considerable literature. Andrews (1980) proposed that final slip function is fractal, and conjectured that the value of the exponent γ equals 2. When discussing this question it is convenient to use the Hurst exponent H instead of γ, because H is the same both for 2D function and for its 1D section, whereas γ is different, being $0.5 + H$ in 1D and $1 + H$ in 2D. Thus, the Andrews guess is $H = 1$. Yin and Ranalli (1995) found that spectra of earthquake surface slip data determined in the field (1D data) agree with the fractal hypothesis and have power-law shapes that give $H \approx 0.2$. From seismologically inverted slip distributions, H was estimated to be in the range 0.7–1 (Tsai, 1997b; Somerville *et al.*, 1999; Mai and Beroza, 2002) (in the last case, the log–log slope of HK tail value is considered); thus γ in 2D is 1.7–2.0;. However, Lavallee *et al.* (2006) noted that HK components of inverted slip maps may be systematically underestimated, either because of constrained overdamped inversion or directly by filtering or smoothing. They arrived at log–log slopes of k spectra that are equivalent to the estimates of H in the range -0.15 to $+0.35$ with mean value around $H = 0.0$–0.1, in better agreement with field data. This result can be considered arguable from the theoretical viewpoint: Mai and Beroza (2002) note that, in the truly fractal case with $H < 0.5$, static self-energy of the fault diverges. This controversy may be apparent, however, and understood merely as an indication that the power-law spectral behavior with $H \approx 0$ must have a definite high-wavenumber limit ("upper fractal limit"). From this discussion, a preliminary guess and the accepted default value is selected as $\gamma = 1.2$.

Another important point is the probability distribution for the individual values M_{0i} of simulated seismic moment of individual subsource. For this variable, abbreviated to M_1, it is assumed that the distribution is lognormal with parameters $(m, \sigma_{\ln,xy})$, with probability density (PDF):

$$p(\ln M_1) = N\left(m, \sigma_{\ln,xy}\right); \; p(M_1) = \frac{1}{(2\pi)^{0.5} M_1 \sigma_{\ln,xy}} \exp\left(-\frac{(\ln M_1 - m)^2}{2\sigma_{\ln,xy}^2}\right) \quad (10)$$

with median value for M_1 equal to $\exp(m)$, mean value $\exp(m + \sigma_{\ln,xy}^2/2)$, and coefficient of variation (standard deviation/mean) $\mathrm{CV}_{xy} = \left(\exp\left(\sigma_{\ln,xy}^2\right) - 1\right)^{0.5}$. Note that, at small $\sigma_{\ln,xy}$, $\mathrm{CV}_{xy} \approx \sigma_{\ln,xy}$. The choice of the lognormal law for final slip map guarantees positivity and provides good control of the variability of M_1. The numerical value of $\sigma_{\ln,xy}$ defines how heavy the upper tail of the distribution of M_1 values will be, i.e., how pronounced the "slip asperities" will be.

At $\sigma_{\ln,xy} > 1$–1.2, one obtains a distribution that is asymmetric, with a rather heavy upper tail; it is clearly non-Gaussian and is associated with powerful asperities. At low $\sigma_{\ln,xy} = 0.1$–0.4, slip distribution is nearly symmetric and nearly Gaussian; the case $\sigma_{\ln,xy} = 0$ is the deterministic constant-final-slip case.

Recently Mai (2004) compiled many observed slip inversions in a convenient standard format as an online database (SRCMOD); this facilitated the comparison of the lognormal law to observational data. Examination of this data set reveals its inhomogeneity, related to the differences of both data quality and resolving power, and also of general concepts and details of the inversion methods used. To establish the distribution law, best quality data with minimum artificial additional correlation must be used. How to formalize selection of such a subset of data is unclear; thus the actual selection of the used subset was subjective. Six inversions of six events were selected, three for crustal and three for subduction earthquakes. To verify the applicability of the lognormal law, each slip map matrix was normalized to its average, and the $\sigma_{\ln,xy}$ parameter was fitted to the histogram data. The result was analyzed by informal comparison of histograms to calculated probability density functions (PDF). Also, the fit for the largest values of slip was tested, comparing empirical and calculated complementary cumulative distribution functions (CCDF). The results are seen on Fig. 3. One can see that, whereas the general fit of empirical histograms to calculated PDFs is reasonable, certain deviations occur. Still, these deviations do not look systematic and repeatable from event to event. Comparison of upper tails of the empirical distribution to the calculated ones is also encouraging. The values of the estimated $\sigma_{\ln,xy}$ parameter are in the relatively narrow range 0.7–0.9, with average value 0.8. From a theoretical viewpoint, the width of the distribution as expressed, e.g., by the value of $\sigma_{\ln,xy}$ should increase with the number of subsources, but this tendency is hardly noticeable among the inverted slip maps, and it seems premature to include this kind of adjustment into simulation.

It should also be noted that, with the present data, the selection of a particular distribution law is highly nonunique. For instance, the quality of fit by means of the Weibull law with parameter 0.85 is similar to that for the lognormal law with parameter 0.80. It should be kept in mind that M_0 estimates for individual cells of fault models used in inversions are not the results of direct experiments, and they bear a significant imprint of inversion procedure. Also, some inversions permit zero M_0 values, while other do not; often these estimates are correlated, and sample sizes are always small. This means that the discussed statistical analysis is unable to produce really accurate estimates and should be treated as mostly exploratory. For the limited aims of simulation of strong motion within the proposed approach, our actual choice of the lognormal law looks justified. Note that both theoretical representations of the observed distributions mentioned above are not strongly heavy-tailed ones; the actual upper tails deviate only moderately from those of the Gaussian law. As the final recommended default value/blind choice for $\sigma_{\ln,xy}$ to be used in simulation, I select $\sigma_{\ln,xy} = 0.90$ estimated over a larger subset of SRCMOD data.

The described description of probabilistic properties of slip can be compared with the results of Somerville *et al.* (1999), who parameterized the distribution of slip in another way. They found that the combined relative area of slip asperities S_a, if defined as the part of the fault area where slip is 1.5× (average slip) or above, covers about 25% of the total fault area (18.4%), with average slip $\overline{D_a}$ over the "highest" 25% of area being about 2.0 times (2.36 times) the average slip $\overline{D}$. In braces, the values are given for the case of the lognormal law with $\sigma_{\ln,xy} = 0.90$; the match was considered acceptable.

As the realistic $\sigma_{\ln,xy}$ values are moderate, one can simplify the simulation by assuming that correlation properties (and thus power spectra) of 2D fields of M_1 values, on one side, and $\ln M_1$ values, on another side, can be treated as analogous. The actual simulation algorithm operates in the following steps. (1) Create white 2D field: stationary random (=uniform) white Gaussian 2D field $A(x, y)$ is generated within a limited piece of the unbounded (x, y) plane, namely over a square of size $Q \times Q$ ($Q > L$, $Q > W$); the result can be visualized as a doubly periodic function (with periods Q and Q) or as a function defined on a torus. (2) Filter: $A(x, y)$ is Fourier-transformed to the (k_x, k_y)

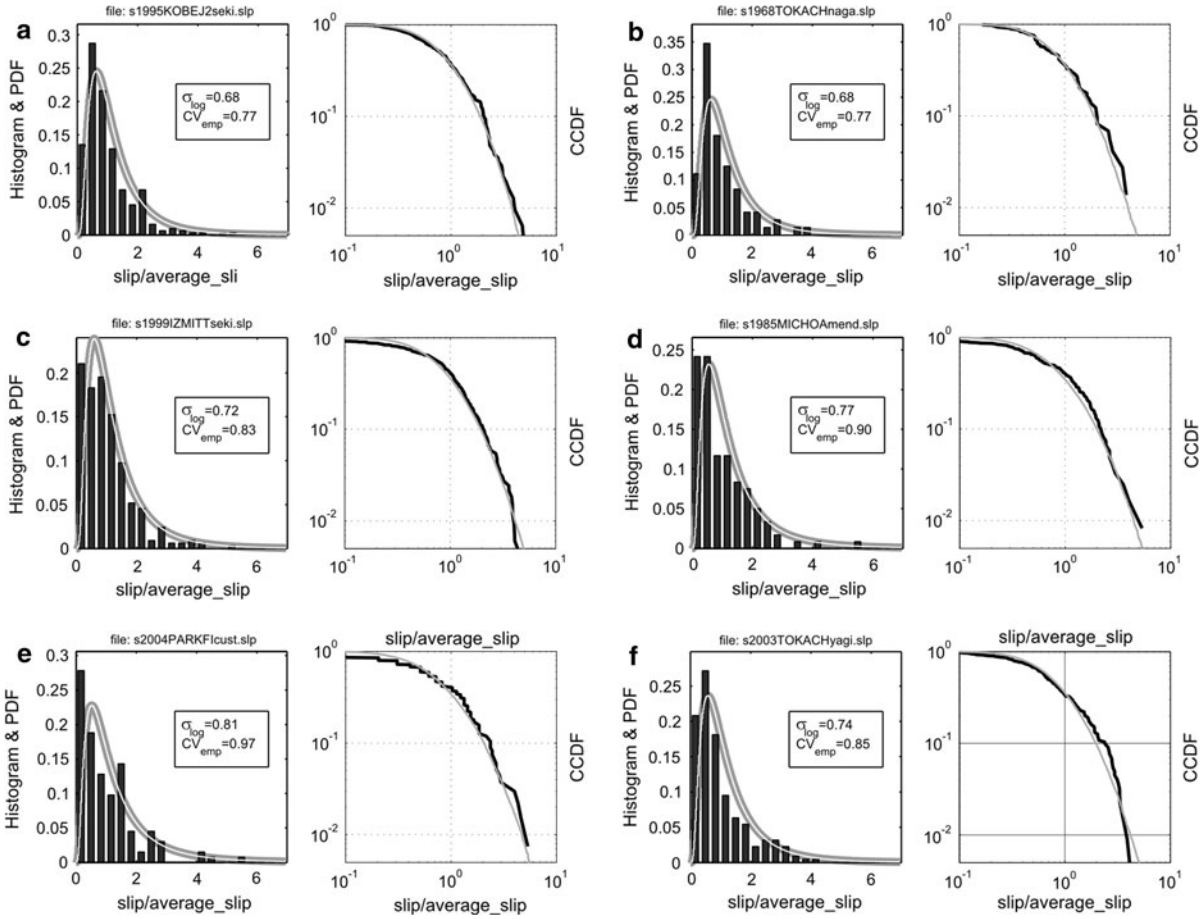

Figure 3

Pairs of plots representing probability distributions of normalized fault slip. In each pair, the *left plot* is the histogram (*bars*) and the right one is the complementary cumulative distribution function (CCDF, *solid line*). Smooth theoretical lognormal PDF and CCDF graphs (*grey*) accompany the empirical ones; these are calculated from the fitted estimates of the $\sigma_{\ln,xy}$ parameter given in the box; CV is the coefficient of variation for the same data. Data of slip inversions were compiled by Mai (2004); the events and references to original source are as follows: **a** 17/01/1995, Kobe (Sekiguchi *et al.*, 1996); **b** 16/05/1968, Tokachi-oki (Nagai *et al.*, 2001); **c** 17/08/1999, Izmit (Sekiguchi and Iwata 2002); **d** 19/09/1985, Michoacan (Mendoza and Hartzell 1989); **e** 28/09/2004, Parkfield (Custodio *et al.*, 2005); **f** 25/09/2003, Tokachi-oki (Yagi, 2004)

domain, "colored" by multiplication by $k^{-\gamma}$ (9) and returned to the (x, y) domain, obtaining $B(x, y)$; Gaussianity is preserved. (3) Obtain the positive non-Gaussian field: $B(x, y)$ is exponentiated to produce a segment of stationary field $C(x, y)$ over $Q \times Q$ with the required PDF (10). The $C(x, y)$ function is a preliminary version of the M_{0i} distribution.

With $C(x, y)$ at hand, one has to pass to definition of the field over the limited $L \times W$ rectangle. The simplest way to do this is merely to make a cutout of the size $L \times W$; this is equivalent to the application of 2D boxcar window function. This mode is however doubtful, for two reasons. First, there are considerable chances that, on such blind cutting, the largest "hill" of the slip function may occur close to or just on the side of the rectangle. As our understanding of real slip distributions is limited, two options are possible in our algorithm: to ignore the possibility of such very asymmetric peaks, or to suppress them. In the latter case, the following technique is used. Assuming $C(x, y)$ to be defined on a torus one can cyclically rotate it along x and along y in such a manner that "hills" have minimal chance to appear on the edges of the selected $L \times W$ rectangle (cyclic rotation preserves amplitude spectrum).

Having thus generated the field over the $L \times W$ rectangle, one meets the second difficulty. As is well known, application of a boxcar window to a stationary process or field significantly distorts the spectrum. The particular kind of distortion is strong high-wavenumber contamination of the spectrum. In the time domain, effects of such a distortion are evident in far-field displacement "source time functions" generated by HASKELL (1964) source as unrealistic, abrupt "starting" and "stopping" phases. As usually done in such cases, I apply a "cap-like" tapering window to prevent these effects. The particular cap shape function along the x coordinate adopted in our algorithm is

$$f(x/L) = f(u) = (u(1-u))^g \qquad (11)$$

and similarly along y, with W used instead of L. For use with a discrete grid, this expression is slightly modified so as not to generate zero amplitudes along the perimeter. The parameter g controls the smoothness of the cap edge; its choice permits one to set: (1) the half-ellipse expected in the case of constant-stress-drop crack, at $g = 0.5$; (2) a bell-like shape at $g \geq 2$; and (3) an approximately parabolic "hill" ($g = 1$) in acceptable agreement with the recent results of MANIGHETTI *et al.* (2005). This detailed empirical study suggests, however, that preferred cap shape function may rather be asymmetric, in contrast with the symmetric shape (11). It must be noted in this relation that the symmetry of the envelope function (11) by no means directly dictates the symmetry of individual random realizations. Whether the option of asymmetric envelopes of simple parametric form is critical for realistic simulation is not clear. At any rate, the degree of variability provided by (11) or its simple generalizations may in many cases be generally insufficient. To provide more versatility, our procedure permits external definition of the M_{0i} distribution, in two possible modes. In one mode, the entire M_{0i} distribution is fixed, permitting no random variability; this case is useful when testing the procedure with earthquakes whose slip distribution can be considered known from independent inversion. In another mode, only the preset window function is set externally, to be used instead of (11) as modulating function and further combined with simulated stationary random field.

A significant problem is how to simulate realistically the slip distribution as a function of dip. SOMERVILLE *et al.* (1999) show an impressive variety of inverted vertical marginal slip distributions that do not support any simple rule. What seems definite, however, is that, for surface-rupturing faults, there is no clear systematic increase of slip at small depths, whereas such an increase can be expected on the basis of the free boundary condition along the upper edge of the fault rectangle for the case of approximately uniform stress drop. Thus, one seemingly need not use different simulation approaches for the cases of buried and surface-rupturing faults. Still, an option is provided in the procedure to remove the condition of zero values of slip along the upper boundary of surface-rupturing fault. An example of simulated slip or M_{0i} map is given on Fig. 4.

3.5. *Simulation of Rupture Front Propagation History*

Rupture propagation is assumed to nucleate at a particular point subsource that is selected as the nearest one to the preset hypocenter location. To select the hypocentral location one can use, e.g., the results of MAI *et al.* (2005), but this approach is not formalized within the described procedure. The fault-average rupture velocity v_{rup0} is found based on the preset average S-wave velocity c_S of the medium (vertical nonuniformity of S-wave velocity is ignored here and throughout entire fault simulation) and the preset value of fault-average Mach number (default value 0.7):

$$v_{\mathrm{rup0}} = \mathrm{Mach}\ c_S. \qquad (12)$$

Two modes of rupture front simulation are provided: circular fronts and arbitrary fronts. In the simpler, circular mode, rupture propagation is assumed to take place radially in constant-velocity steps, with each step covering distance d_{sub}. For each step between successive circles of radius id_{sub}, $i = 0, 1, 2\ldots$, a random value of local rupture velocity v_{rup} is generated. These values are assumed to be independent, with mean v_{rup0} and uniform probability distribution around v_{rup0}, in the range $[(1 - D_v)\ v_{\mathrm{rup0}}, (1 + D_v)\ v_{\mathrm{rup0}}]$. The relative half-width parameter D_v is a preset constant. In the present version,

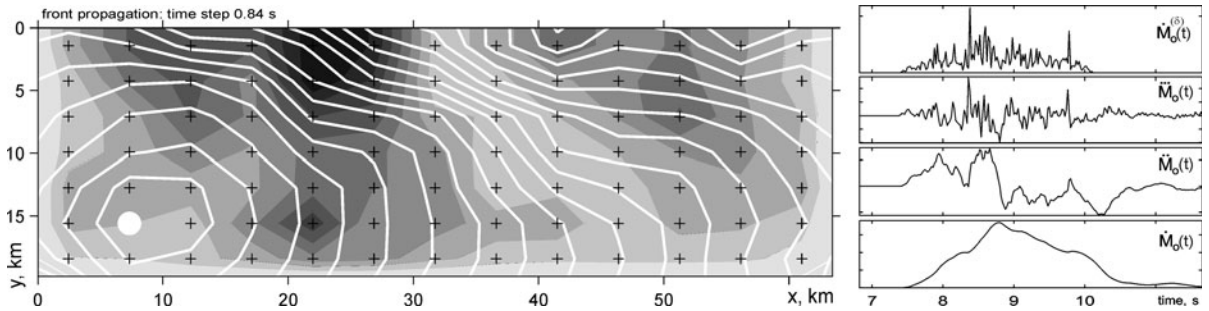

Figure 4

Left an example simulated 2D final slip function. Its amplitudes are depicted as shades of *grey*; the maximum (*black*) reaches 5.3 m. Fault parameters: $M_w = 7.2$, $L = 63$ km, $W = 20$ km. Subsource grid 13×7 (*crosses*). Random slip follows isotropic $k^{-1.5}$ wavenumber amplitude spectrum. Two-dimensional taper function used over three sides; the upper side ($y = 0$) is assumed to cross the Earth surface and is not tapered. *White dot* is the nucleation point. *White contours* are successive rupture front positions, simulated kinematically from random rupture velocity field. *Right* example time histories associated with a particular subsource. Upper trace is the preliminary time history $\dot{M}_{0i}^{(\mathrm{PRF})}(t)$. Three other traces are seismic moment time history derivatives $\dddot{M}_{0i}(t)$, $\ddot{M}_{0i}(t)$, and $\dot{M}_{0i}(t)$; they represent the subsource contribution to far-field body wave acceleration, velocity, and displacement, respectively

rupture is not permitted to stop or to decelerate strongly, and the lower-bound value of local velocity, of the default value 0.3 km/s, is also preset (this is a disputable decision, however, because double earthquakes are a real fact). As a result of this construction, rupture propagation history along radius is determined. This time history is essentially a linear trend perturbed by Brownian motion. Interpolating this function, the rupture arrival time is defined for each point subsource, which is assumed to be located in the center of a cell. When all cells are covered, the total rupture propagation time T_{prop} is calculated as the maximum among these onset times.

In a more advanced mode, the 2D distribution of random values of v_{rup} controls the front propagation history. This simulation also follows a kinematic approach, and no dynamics is involved. The rupture front history is simulated departing from a stochastic rupture velocity field on a fault. Having constructed such a field, the rupture front evolution is modeled from its beginning at nucleation point or hypocenter and until the entire fault surface is ruptured. Evolution takes place according to the Huygens principle; that is, each grid node on the front of a rupture that fails at a certain time moment is considered as a source of a "signal to rupture" that arrives at all neighboring nodes with delay defined by the local v_{rup} value. The value of discrete step along distance is adjusted automatically during simulation to prevent problems with singularities of front geometry. The distribution of rupture velocity values $v_{\mathrm{rup}}(x, y)$ over the fault is generated in a manner similar to one used for slip distribution. First, a discrete 2D Gaussian random field is generated with a definite power spectrum, which again is assumed to be power-law in wavenumber. Correlation properties of this field are defined implicitly through this power spectrum (note that, for such a field, there is no well-defined correlation length). This field cannot be directly used as a set of local rupture velocity values because its values have a Gaussian distribution, and in such a case, a certain fraction of negative or too high velocities are generated. To amend this deficiency, Gaussian-distributed values are further replaced by values from another distribution, more appropriate for rupture velocities; in this transform, the rank of the value within the variational series is preserved. In the actual algorithm, the uniform distribution is used. As a result, low values of the original field are transformed to low values of the output, and high values as well, but inadequate negative or high positive values of velocity disappear. Such a procedure permits one to change the distribution law while preserving, approximately, the spatial correlation properties (in fact, passing from the Gaussian to the lognormal law for slip rate, used in the previous section, represents a replacement of a similar but technically more simple character). To suppress distortions related to simulation grid discreteness, rupture front propagation is first traced over a denser

grid, and the resulting grid of arrival times is rarified afterwards. Through the use of various degrees of spatial correlation controlled by the exponent of the power law, and various distributions of individual velocity values, a wide degree of front propagation styles can be imitated, from nearly circular to rather erratic. Note that using *correlated* velocity field is a must: uncorrelated ("white") random velocity field produces only slightly perturbed, nearly circular fronts. An example simulated rupture front propagation history is given in Fig. 4.

3.6. Simulation of Preliminary Time Histories of Each Subsource (Preliminary Source)

The set of time histories of subsources is a main tool to express the application-oriented description of the earthquake source process proposed in the present paper. They can be viewed as consisting of two components: low-frequency and high-frequency ones. The low-frequency part (the component observable at low temporal resolution), describes systematic local slip rate evolution, with smooth time histories whose shape is well correlated from point to point. If one suppresses rupture front and slip distribution randomizations, the low-frequency fault behavior becomes simple and deterministic. The high-frequency component of subsource time histories represents random individual features of local slip; in the simplest simulation mode they are uncorrelated from point to point. Physically, HF time histories play two roles. First, they describe time history of slip averaged over a subsource cell, i.e., true time history of subsource seismic moment rate. Second, they represent the seismic energy that is created by the variability of fault motion over small spatial scales, from the subsource size and lower. Indeed, the simulation is based on an artificial construction when all points over a subsource cell move in phase, and this inaccuracy must be corrected. By cutting the wavenumber spectrum of the final slip distribution at wavenumber $1/d_{\mathrm{sub}}$, effects of spatial, HK structure of slip rate become unobservable, and a significant source of HF seismic energy is artificially suppressed. The scheme with fitting of far-field spectra (see later text) is essentially a tool to bypass the arising problems. When one applies changes, e.g., reducing d_{sub}, the balance of energy between the described components changes, but the summary far-field spectrum is preserved (random scatter aside).

The length of the time window with nonzero $\dot{M}_{0i}(t)$ is related to T_{rise}; it is either equal to it, or may be somewhat larger when an asymmetric envelope shape is assumed. Technically, $\dot{M}_{0i}(t)$ is simulated over a time interval of duration $T_{\mathrm{loc}} = (1.0\text{–}2.5)T_{\mathrm{rise}}$. To represent the broadband radiation that occupies this interval, as a first step, positive stationary random noise is generated that fills the mentioned window. Eventually, this noise will be transformed into the HF component of a final time history. A significant step in simulation planning is to choose the probability distribution law of noise amplitudes.

There is almost no theoretical consideration regarding such a choice, and the law must be selected on the basis of limited empirical information. An important piece of information is the probability distributions of peaks of near-source accelerograms and other HF signal amplitudes. It was noted in the "Introduction" that such distributions are usually heavy tailed, with enhanced probability of large deviations; this makes a signal trace look "spiky". The upper tail of the complementary cumulative distribution function in such a case is often approximated by the power law: $\mathrm{Prob}(x > x') \propto x^{-\alpha}$, where the exponent α is the key parameter describing upper tail behavior (the standard example is the hyperbolic or Pareto law). Gusev (1989) suggested that near-fault acceleration peaks have a heavy-tailed non-Gaussian distribution with power-law upper tail, and proposed the value $\alpha \approx 2$ (that looks too low at present). Gusev (1992) came to the estimate $\alpha = 2.3$, obtained from the peak-to-rms amplitude ratio of teleseismic HF amplitudes. Gusev (1996) analyzed empirical distributions of peaks of 32 records of large-magnitude Mexican earthquakes obtained at distances of 30–100 km, revealing rather reliably the heavy-tailed behavior for accelerogram amplitudes. The simplest accelerogram model, that of a segment of stationary Gaussian process, was found to be completely invalid for these data. However, the degree of heavy-tailed behavior found in this study is rather moderate, as expressed by the estimate $\alpha = 5$. The degree of spikiness of an accelerogram decreases with increasing hypocentral distance,

because scattering along the path makes the probability distribution of the signal less heavy tailed ("normalization of signal"). Thus, in the immediate vicinity of a fault, and similarly for the radiating spot on a fault, a more realistic interval estimate may be $\alpha = 3$–4. The concept of heavy tails of peaks of HF radiation was recently supported by LAVALLÉE and ARCHULETA (2003, 2005).

In the procedure presented here, the amplitude distribution of a signal generated by a subsource is described by the lognormal law [like (10), but with $\sigma_{\ln,xy}$ replaced by another parameter $\sigma_{\ln,t}$]. The value of $\sigma_{\ln,t}$ defines the degree of spikiness in the same way as $\sigma_{\ln,xy}$ defines the degree of expression of slip asperities. From the technical viewpoint, for samples of limited size such as 100–300, upper tails of a power law and a lognormal law do not differ greatly, and can be matched by accurate selection of parameters. To substantiate our choice, it can be noted that (10) provides a much more realistic description of the central part of the distribution than, e.g., a Pareto law. Also, it seemed conceptually reasonable to unify theoretical probability laws used to simulate source process variability in space and time in a situation where each of them was known with very limited accuracy. It is easy to convert the range of parameter α to the corresponding range of the parameter $\sigma_{\ln,t}$ if certain reasonable interval of quantiles is set. For the selected upper quantile interval of 0.3–3%, the range $\alpha = 3$–4 can be translated to the range $\sigma_{\ln,t} = 0.65$–0.8 for the lognormal law. Our current preferred value, taken as the default, is $\sigma_{\ln,t} = 0.75$, which approximately corresponds to $\alpha = 3.3$. Note that the degree of spikiness that is observed in near-fault accelerograms of real earthquakes varies widely, thus the range $\sigma_{\ln,t} = 0.6$–1.1 may serve as a reasonable starting approximation to parameterize its variability.

GUSEV (1989) and LAVALLÉE and ARCHULETA (2005) related heavy-tailed probability distributions of acceleration to similar distributions of local stress drop over a fault, or stress-drop asperities. This may be a correct idea in general, but it should be understood that prominent spikes can be also generated by another mechanism, through constructive interference of parts of the rupture front (see OGLESBY and ARCHULETA, 1997 for a good example), thus representing a dynamic phenomenon not immediately reflected in the static features such as the local stress drop distribution over a fault. Taking such a possibility in consideration, one has to accept that the description included in the simulation procedure is to a large degree a phenomenological one; still, this does not undermine the assertion that the approach developed here is able to represent some key probabilistic accelerogram properties realistically.

To simulate local slip rate/subsource moment rate time history as random signal over a finite time segment, using the lognormal probability distribution, the construction used is similar to one that was already used for generating 2D function of final slip, but in one dimension, t, only. At the first stage, positive stationary signals are generated over a time segment of appropriate duration, with lognormal probability distribution and typically no correlation (discrete white noise). It was noted that weakly correlated signals with "pink," not white power spectrum were slightly more efficient, producing fewer artifacts; but, from the general viewpoint, details of these spectra are of no real importance, as the general shape of amplitude spectrum will be radically modified at the later stage. To obtain nonstationary finite-duration signal, the crude stationary signal is multiplied by an envelope shape function (modulated). In the actual implementation of the algorithm, the envelope-shape function can be chosen out of several preselected families. The two main options are: (A) a symmetric "cap-like" shape identical to (11), boxcar case included; (B) smoothed $t^{-0.5}$ hyperbola, expressedly asymmetric with slowly decaying tail (truncated). Shape A generalizes the HASKELL (1966) model with ramp-like slip function; this option may be sufficient in most cases. Shape B imitates the crack-tip behavior, modified for the case of finite cohesion zone, and is included mostly to follow tradition.

After the modulation stage, each subsource time history is rescaled to set its integral equal to already known subsource seismic moment M_{0i}, and finally delayed by the rupture propagation time for the subsource in question. The result represents preliminary local slip/subsource seismic moment time history, denoted $\dot{M}_{0i}^{(\mathrm{PRE})}(t)$. Note that, at the modulation stage, the modulation/envelope function is smooth and nonrandom, whereas the mean value of the positive

stationary noise is constant in time. Therefore, the set of envelope functions (replicated, weighted by M_{0i}, and time-shifted at each subsource) directly represents the low-frequency deterministic component of local slip rate time history over the entire source.

The set of $N = n_x \times n_y$ $\dot{M}_{0i}^{(\mathrm{PRE})}(t)$ functions (in units of seismic moment rate) represents a complete description of the space–time structure of the preliminary source. The sum or stack of all individual time histories is denoted $\dot{M}_0^{(\mathrm{PRE})}(t)$, and its amplitude spectrum $|\dot{M}_0^{(\mathrm{PRE})}(t)|$ is the preliminary "source spectrum," or Fourier spectrum, of the moment rate time history of an equivalent point source. Examples are given of individual preliminary time history of a subsource in Fig. 4, and of a complete set $\dot{M}_{0i}^{(\mathrm{PRE})}(t)$ in Fig. 5.

A significant conceptual deficiency of the above-described algorithm is its inability to create a credible spatial correlation of HF signals. In the described mode of simulation, the HF temporal structure of source development is assumed, by construction, to be completely uncorrelated between subsources (no correlation between pairs of time histories), but, implicitly, completely correlated within the subsource area (complete correlation between time histories for two spots on the same subsource cell). Thus, the source is incoherent in a certain sense, but this incoherency is frequency and wavenumber dependent in an intricate way. In addition, the properties of incoherency depend on the selection of the d_{sub} parameter, which is assumed to play only a technical role in our simulation procedure. Sometimes this may be tolerable, but a more general approach is clearly needed. To improve this situation one might use a fault model with frequency-dependent correlation length as proposed in (Gusev 1983). A particular procedure was designed that adds the needed kind of correlation between pairs of subsource time functions; it was incorporated into the PULSYN2008 code and is described in the next section. After this adjustment, one can expect to obtain much more reliable results at small fault-to-receiver distances. Generally, if one can trust the assumed random space–time fault structure, it becomes possible to simulate fault motion in arbitrary detail, and ground motion at an arbitrary small fault-to-receiver distance.

3.7. *Creating Random Subsource Time Functions with Appropriate Spatial Correlation Properties*

In simple incoherent source models (Blandford, 1975; Hanks, 1979; etc.) all HF subsources are assumed statistically independent, their time histories uncorrelated, and their energy contributions additive.

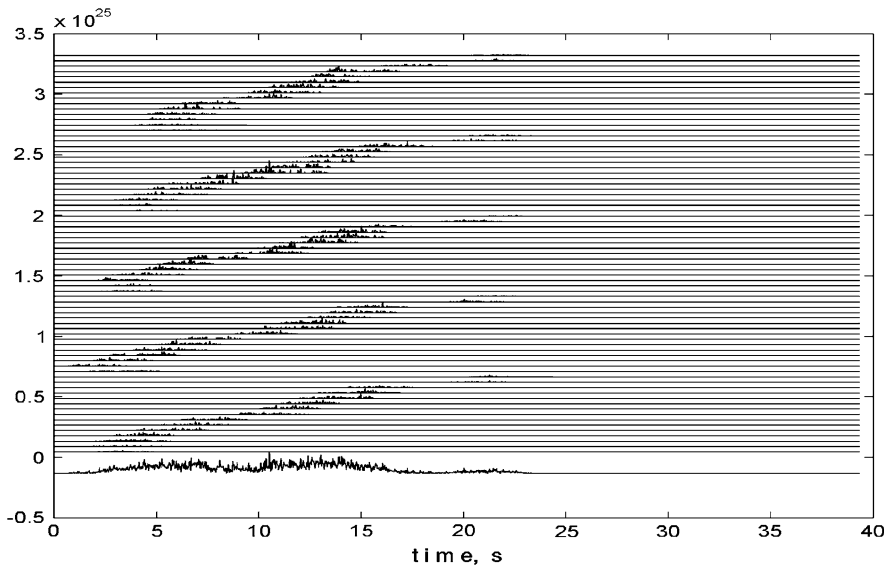

Figure 5
Preliminary time histories $\dot{M}_{0i}(t)$ for each of the 91 subsources of Fig. 4. The lowermost trace is the sum over all subsources. See Fig. 4 for an example of single-subsource $\dot{M}_{0i}(t)$

This is a good starting idea, but insufficient to relate local slip rate amplitudes consistently to source radiance flux. The way to overcome this difficulty was proposed by GUSEV (1983), who noted that a reasonable requirement for a stochastic earthquake source considered as a HF S-wave radiator is that its correlation radius r_c for motion within a given frequency band around f be comparable to the corresponding wavelength $\lambda = c_S/f$. Of course, if such a radiator is forced externally, any fine details can be imagined to be present in its spatial structure. The effect of such details, however, will be localized and manifest itself only in the static field; in other terms, only inhomogeneous nonradiating "waves" will be generated. Thus, this small-scale motion, if real, is near to unobservable even in this case. However, one can expect that, for an indigenous source created by elastic rebound, the assumption that correlation length $d_c = 2r_c$ equals λ (or maybe greater) is a reasonable starting approximation (the case $d_c > \lambda$ deserves attention in the future). To describe a source with such properties in a primitive way, GUSEV (1983) proposed that, at any given f, the fault can be thought to consist of many independently radiating spots of size $d_c = \lambda$, and managed to relate fault motion and far-field radiation field of HF source in a band around f. Let us call the frequency-dependent spots of (GUSEV, 1983) "λ-spots." Note that entire further discussion regards only HF, noise-like component of fault radiation. In the following, we must accurately distinguish between a "numerical" subsource, i.e., point source in the center of a fault cell, and the corresponding square cell of the original fault model, with continuous slip rate over (x, y). Denote these entities as δ-subsource and cell-subsource.

There is important difference between the mentioned theoretical case, where the size of a spot is frequency dependent, and the numerical procedure described earlier, where mutually independent subsources of a fixed size generate entire HF spectrum with a wide set of wavelengths. Consider first the case of frequency band of radiation with very small wavelength $\lambda_1 \ll d_{\mathrm{sub}}$ (very high frequency f_1). Then each cell-subsource consists of many incoherently radiating λ-spots whose summary effect is correctly deduced from far-field spectrum; thus the time function for the corresponding δ-subsource will be adequate, and no problems arise. In the opposite case of moderate frequency f_1 (still within the HF range), and much longer wavelength $\lambda_2 \ll d_{\mathrm{sub}}$, the assumption of uncorrelated time functions becomes evidently invalid. To rectify this situation it is sufficient to impose a correct degree of spatial correlation on the time histories of subsources. After such adjustment, no principal problems are seen for application of our procedure in the vicinity of a fault.

As an input for the algorithm that performs the described task it was convenient to use the spatially uncorrelated output created in the previous section. To modify it appropriately, the following straightforward sequence was implemented: (1) For each subsource, take the given space–time signal along time axis, and break it down in the frequency domain into the set of band-limited signals, each with well-defined central/characteristic frequency. (2) For each frequency band, and each moment of absolute time, perform smoothing along spatial axis or axes, applying an appropriate spatial filter; the width of pulse response (correlation length) should be equal to the wavelength defined by the central frequency of the corresponding bandpass filter. No processing is needed for signals with wavelengths below d_{sub}. (3) For each subsource, sum the results over all bands, recovering the broadband frequency spectrum. These operations are made with normalized signals (each with unit integral); the nonuniform spatial structure expressed as the set of M_{0i} is suppressed before the described procedure and recovered after it.

Figure 6 illustrates this approach for the case of stationary, identical-rms-amplitude signals generated by means of the described procedure for the case of a single spatial dimension from a discrete white input. A string of 100 subsources is situated along the x axis at the interval 0.63 km, the time span considered is 16 s, and the uppermost considered frequency is 8 Hz. Two pairs of pictures are shown for the two particular bands cut out of the original input, with central frequencies 2.8 and 0.7 Hz; the corresponding correlation distances are 1.25 and 5 km, respectively. One plot in a pair depicts the space–time signal before imposing correlation structure; the other shows the result of spatial smoothing. Broadband signals are not shown because, after summation over

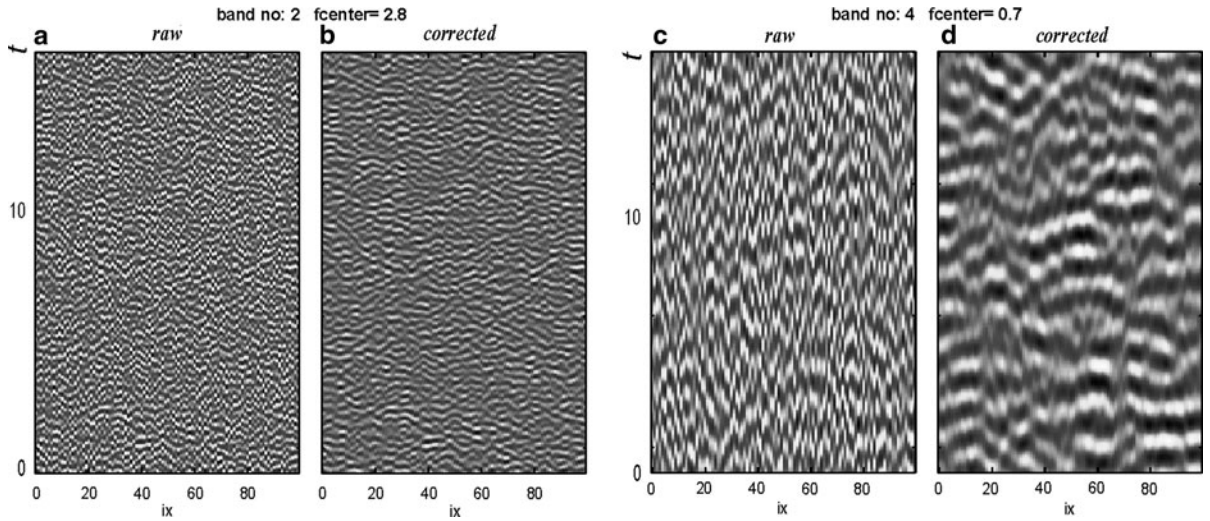

Figure 6
Simulated example traces of slip rate in time (along ordinate, *s*) for a line of hypothetic subsources (along abscissa, step 0.63 km, numerals are sequential numbers of subsources). *Graphs* are given for two frequency bands: 2.8 Hz (**a**, **b**) and 0.7 Hz (**c**, **d**); shades of *grey* indicate amplitude. Raw traces (**a**, **c**) are uncorrelated between subsources; adjusted traces (**b**, **d**) have correlation lengths close to wavelength

bands, the fine correlation structure created in the described way becomes visually indiscernible.

3.8. Defining the "Target" Amplitude Spectrum

The preliminary space–time description of the source as $\dot{M}_{0i}^{(\mathrm{PRE})}(t)$ should be modified, so that the spectra of our final simulated source time functions follow a well-established spectral scaling law, acceptable for the region of study. One might use smoothed average empirical spectral shapes as they stand, like the semi-empirical scaling law of Gusev (1983), or parametric descriptions of spectral shapes. However, the difference is not great because, through increasing the number of parameters, one can approximate rather complicated empirical laws (see, e.g., Koyama, 1985). The common approach is the use of the scaling law of Brune (1970) in its simplest single-corner form. Arguments have been presented that such a description is, generally, oversimplified. A number of options are implemented in the described simulation procedure, among them: (1) scaling of Gusev (1983), tabulated, with no similitude of spectral shapes (somewhat outdated but often useful); (2) Brune's (1970) formula with $\varepsilon = 0$, as a three-parameter (L, W, $\Delta\sigma$) modification of Joyner (1984), who tried to account for elongated source shape; and (3) the four-parameter 2-Brune formula of Atkinson (1993), which can describe spectral scaling laws both with and without similitude; its use will be illustrated among the examples of application of PULSYN below. Also, tabulated target spectrum or entire tabulated scaling law can be set externally.

Brune's analytical spectral shape is known to be of limited accuracy just at the spectral corner (e.g., a simple isosceles-triangular pulse makes the first spectral hole just at the position of the corner defined by its HF spectral asymptote). Such problems are absent from the present technique, as the entire spectral band from $f = 0$ to $f = (4\text{–}6)f_c$ is formed on the basis of the independently simulated LF rupture history, and the target spectrum is mostly ignored here. In this band, all deviations from the standard scaling law that are related to variations of average rupture velocity or to the difference of propagation time in unilateral and bilateral rupture modes are accounted for automatically.

For the case of a typical stress drop ($\delta = 0$), one can use target spectra taken directly from the mentioned spectral families. In order to adjust target spectral shape to account for nonstandard stress drop, the δ parameter can be used. For a given M_w and M_0 value, denote the "reference" values of f_c and $\Delta\sigma$ for the standard case of $\delta = 0$ as $f_{c\ \mathrm{ref}}$ and $\Delta\sigma_{\mathrm{ref}}$.

Generally, the assumption of scaling predicts that $\Delta\sigma \propto M_0 f_c^3$. As $\Delta\sigma = \Delta\sigma_{\mathrm{ref}} 10^{\delta}$, one can write

$$f_c(M_0, \Delta\sigma) \propto M_0^{-1/3} \Delta\sigma^{1/3} = M_0^{-1/3} \Delta\sigma_{\mathrm{ref}}^{1/3} 10^{\delta/3}. \quad (12)$$

Therefore, for a parametric spectral law, to scale spectrum at a given M_0 to nonstandard stress drop case, one should modify the standard f_c value in the following way:

$$f_c(M_0\delta) = f_{c\,\mathrm{ref}}(M_0) 10^{\delta/3}. \quad (13)$$

In the case of ATKINSON (1993) scaling, similar correction may be applied for each of the two characteristic frequencies f_a and f_b.

For a nonparametric, tabulated empirical-average spectral scaling law, a special procedure was proposed by PANZA (1999, pers. commun.), as follows. Given an empirical average scaling law $\dot{M}_0^{(\mathrm{TAR})}(f)$ and nonstandard stress drop expressed through $\delta \neq 0$, one can adopt the spectral *shape* from the "auxillary-reference" ("AU") event, which follows the scaling law, but with another M_0 value (e.g., smaller than given M_0 for the case $\delta > 0$), denoted by $M_{0,\mathrm{AU}}$. This spectrum, with acceptable shape and incorrect absolute level, can further be appropriately scaled to result in the correct M_0 value. For "AU" event with $\delta = 0$, from (13), $f_c(M_{0,\mathrm{AU}}, \Delta\sigma_{\mathrm{ref}}) = \mathrm{const}\ M_{0,\mathrm{AU}}^{-1/3} \Delta\sigma_{\mathrm{ref}}^{1/3}$, whereas for the target event with $\delta \neq 0$ and given M_0, again from (13), $f_c(M_0, \Delta\sigma) = \mathrm{const}\ M_0^{-1/3} \Delta\sigma_{\mathrm{ref}}^{1/3} 10^{\delta/3}$ with the same constant. As the spectral shapes of these two events are assumed analogous, their f_c values can be equated, to obtain

$$M_{0,\mathrm{AU}} = M_0 10^{-\delta}. \quad (14)$$

Therefore, the target spectrum for given M_0 and $\delta \neq 0$ is created in three steps: (1) the reference M_0 value, $M_{0,\mathrm{AU}} = M_0 10^{-\delta}$ is found, (2) from the empirical scaling law the average target spectrum $\dot{M}_0^{(\mathrm{TAR})}(f|M_{0,\mathrm{AU}})$ is extracted, and (3) the result is multiplied by $10^{-\delta}$.

Adjustments that are needed in case of using the second spectral correction δ_{HF} should now be considered. If $\delta_{\mathrm{HF}} \neq 0$, I wish to additionally modify HF spectral level while introducing no changes to the target spectrum in the vicinity of corner frequency. The latter condition is fulfilled automatically however, because target spectrum has no effect on the vicinity of corner frequency: this part of simulated spectrum is shaped by actual simulated rupture history. The value of δ is automatically matched to this history through the following chain: δ value → fault area [through (3)] → fault size → rupture duration → corner frequency. Therefore, to take δ_{HF} into account, it is sufficient to replace δ by $\delta + \delta_{\mathrm{HF}}$ in (13) and (14). In our experience, this simple approach yields sometimes acceptable, but generally insufficient control over the middle part of the spectrum [(2–8)f_c range]; the approach based on the ATKINSON (1993) 2-Brune shape is more efficient, despite its larger number of parameters.

It seems relevant to mention here an important property of the present model. In this model, HF spectral level is not affected by variations of the rupture velocity or of the nucleation point position. It is believed that, despite all such variations, the high-frequency spectral energy density is relatively stable over focal sphere, and is merely smeared over a shorter or longer time interval; the rms level of amplitude spectrum is stable as well. Therefore, no directivity is formed by this model for HF spectral levels, and only weak directivity—for amplitudes (as amplitude ∝ duration$^{-0.5}$). Typically, observations of strong motion show no or weak directivity, at least with respect to spectral levels (TSAI, 1997a; BOATWRIGHT *et al.*, 2002). Properties of macroseismic intensity are similar: directivity effects are seen only infrequently on isoseismal maps. This is in contrast to the source model of a propagating brittle crack or dislocation (both with continuous or random slip). In this case the amount and angular distribution of energy radiated at high frequencies depend very significantly on local rupture velocity, contrary to the above assumption (also cf. DAY *et al.* 2008). I believe that assumptions made regarding this point are acceptable at the present level of knowledge of real fault behavior. Still, some observations suggest that certain enhancement of forward directivity at high frequency sometimes takes place; thus, more general approach may be needed in future, accounting for partial coherence of the source.

The use of a specific regional scaling law is a significant instrument for attaining realistic simulation of ground motions. Clear examples of variations

among regional spectra are those between Eastern USA and Western USA and between reverse dip-slip faults and normal faults. An impressive example of regionally specific spectral parameters is shown by AGUIRRE and IRIKURA (2007). On a subregional scale (PARVEZ *et al.*, 2001), a threefold difference of average peak accelerations and velocities was found between two areas in the Himalayas.

3.9. *Construction and Application of the "Finishing Operator" that Converts the Preliminary Source into the Final One*

In the previous section I have shown how the target spectrum is constructed. I would like to simulate a signal whose spectrum is near to this target. Note that the target spectrum is a smooth function, whereas the spectrum of simulated signal that approximates it is ragged. Thus, they cannot be near in any strict sense, and no more than an approximate match can be provided between the smoothed version of the spectrum of the simulated signal and the target spectrum. This match is pursued only for the $\dot{M}_0(t)$ signal that would be observed on the ray in the direction normal to a planar fault. At any other point on a focal sphere, additional delays appear, resulting in relative squeezing or stretching of far-field wavetrain, corner-frequency variation over the focal sphere (Doppler effect), and, locally, to generation of "forward directivity pulses." However, I believe that, in the empirically based spectral scaling laws, such effects are suppressed by implicit averaging over the focal sphere.

The preliminary source as described by the set of $\dot{M}_{0i}^{(\mathrm{PRE})}(t)$ has correct final slip, rupture front history, and rise time; along the time axis, signal amplitudes are "noisy" and "spiky," as required. In the frequency domain, amplitude spectrum is also nearly adequate at LF, but grossly overestimates the target spectrum at HF [this is the result of selection of white (ω^0) or pink ($\omega^{0.5}$) noise for the HF part of $\dot{M}_{0i}^{(\mathrm{PRE})}(t)$, instead of a "more realistic" amplitude spectral shape such as $\omega^{1.5-2}$]. This part of spectrum must be modified. It can be said that phase spectrum of $\dot{M}_{0i}^{(\mathrm{PRE})}(t)$ functions is almost acceptable, but amplitude spectrum needs significant correction in its HF part. Therefore it is clear that different parts of the spectrum need different treatment. To simplify the further discussion, let us divide the frequency axis into a "very-low-frequency part" (VLF, below $0.5f_c$), "intermediate-frequency part" [IF, $(0.5–5)f_c$], and high-frequency part [HF, above $(4–6)f_c$]. In the VLF part, the match between the target spectrum and the resulting spectrum is attained automatically, through identical M_0 values. In the HF part, the fitting of spectra is a relatively well-posed problem, because the source signal here can be treated as a segment of stationary random noise. Thus, the fit can be attained in a common statistical sense, using rms amplitude spectrum. This rms spectrum can be understood either as a mean, which corresponds to an abstract averaging over a multitude of realizations over sample spectral shapes, or as a result of smoothing of an individual "ragged" spectral shape of a single realization. In the source seismology, one can safely assume the mean-squared amplitude spectrum (or mean energy spectral density) to be a slowly changing function of frequency, and using the usual ergodicity assumption, one can expect that it will match the smoothed (in the rms sense) squared amplitude spectrum of a realization [note that this definition is numerically different from the approach of BRUNE (1970) and his followers: at least in principle, they plotted their generalized smooth spectral shapes as envelopes of deterministic spectra, and not as rms averages of stochastic ones; this results in the numerical difference of approximately 1.4 times, estimated as the difference between mean extreme and rms value for the cases of both a sinusoid and a random Gaussian process]. Therefore, the simulated ("ragged") spectrum of realization must be created in such a way that its smoothed version matches the target spectrum.

As for the IF part, it is very difficult even to formalize what represents a good fit between actual and target spectra, because this is a boundary area between stochastic and deterministic ways of description. Also, as was already explained, target spectrum cannot serve as a good model of a real spectrum in this band. Fortunately, this problem need not be solved at all. In our already constructed low-frequency source model, factors such as source size, rupture velocity, and nucleation point position have already been taken into account. Thus the already

constructed signal and its spectrum can be considered as an adequate approximation. A small problem still remains: how to select the critical boundary frequency separating IF and HF ranges, and to how to "glue" source descriptions smoothly in these ranges.

Let us represent this approach formally. I depart from the smooth target amplitude spectrum $\dot{M}_0^{(\mathrm{TAR})}(f)$ obtained as described in the previous section, and the preliminary signal amplitude spectrum is $|\dot{M}_{0i}^{(\mathrm{PRE})}(f)|$. The low-frequency structure of $\dot{M}_{0i}^{(\mathrm{PRE})}(f)$ needs no adjustment, whereas at HF its level, $|\dot{M}_{0i}^{(\mathrm{PRE})}(f)|$, is too high. To rectify this deficiency, I modify the preliminary time histories by applying a specially designed "finishing operator." In time domain, it reduces to finely tuned smoothing, performed through convolution with a certain pulse of unit integral further called "finishing pulse." The unit value of the integral guarantees that the correct M_0 value of the preliminary source will be preserved. The finishing operator is constructed in frequency domain. The first step in its construction is to smooth $|\dot{M}_{0i}^{(\mathrm{PRE})}(f)|$, applying Gaussian spectral window, giving a new version $|\dot{M}_{0i}^{(\mathrm{PRE},sm1)}(f)|$. The spectral window is designed in time domain: the half-width of its Fourier transform (=pulse response) is set equal to $0.13T_{\mathrm{prop}}$. This choice was defined through trial and error. The aim of this smoothing is to modify $|\dot{M}_{0i}^{(\mathrm{PRE})}(f)|$ so as not to create too precise a finishing operator (which would produce a meaninglessly accurate approximation of the target spectrum). Instead, a more plausible rms approximation will be performed.

Smoothing by finishing operator is needed only over the HF range, whereas in the IF range it is undesirable: the finishing operator must be near unity in this part of the spectrum, where the result is already acceptable; any spectrum smoothing spoils this condition. To provide this behavior, $|\dot{M}_{0i}^{(\mathrm{PRE},sm1)}(f)|$ is further modified in the following way:

$$|\dot{M}_{0i}^{(\mathrm{PRE},sm2)}(f)| = |w_{\mathrm{LF}}(f)|\dot{M}_{0i}^{(\mathrm{PRE})}(f)| + w_{\mathrm{HF}}(f)|\dot{M}_{0i}^{(\mathrm{PRE},sm1)}(f)|, \quad (15)$$

where $w_{\mathrm{HF}}(f)$ is a smoothed step function increasing from zero at $0.3/T_{\mathrm{prop}}$ to unity at $7/T_{\mathrm{prop}}$, and $w_{\mathrm{LF}}(f) = 1 - w_{\mathrm{HF}}(f)$. The boundary point where $w_{\mathrm{LF}}(f) = w_{\mathrm{HF}}(f) = 0.5$ corresponds approximately to $0.13f_c$; this value, and the particular shape of the tapering function $w_{\mathrm{HF}}(f)$ function were selected by trial and error. Note that summation in (15) is applied to signals originated as a set of broadband $\dot{M}_{0i}^{(\mathrm{PRE})}(t)$ functions, thus no problem of temporal mismatch between LF and HF summands can arise.

Now I can construct the sought "finishing operator"; its modulus in frequency domain is

$$|U(f)| = \left|\dot{M}_0^{(\mathrm{TAR})}(f)\right| \Big/ \dot{M}_0^{(\mathrm{PRE},sm2)}(f). \quad (16)$$

Its phase spectrum is then added, in the simplest case so as to make it causal (minimum phase). This procedure is illustrated in Fig. 7. Finishing operator is shown in frequency domain in Fig. 5b, and in time domain (finishing pulse) in Fig. 7d, marked "D" on both graphs; it converts $\dot{M}_0^{(\mathrm{PRE})}(f)$ to final source spectrum $\dot{M}(f)$. Operators marked "V" and "A" convert $\dot{M}_0^{(\mathrm{PRE})}(f)$ to $\ddot{M}_0(f)$ and $\dddot{M}_0(f)$. From spectral plots one can see that use of unsmoothed $\dot{M}_0^{(\mathrm{PRE})}(f)$ in (16) would make the resulting spectral shape accurately copy the (smooth) $\dot{M}_0^{(\mathrm{TAR})}(f)$ spectrum in the HF part; the actual algorithm results in much more realistic, "ragged" spectrum (actually, however, it is still too near to $\dot{M}_0^{(\mathrm{TAR})}(f)$; this problem is discussed later).

The finishing operator (i.e., convolution with finishing pulse) is applied to each of preliminary subsources $\dot{M}_{0i}^{(\mathrm{PRE})}(t)$, giving a final set of time histories $\dot{M}_{0i}^{(\mathrm{FIN})}(t)$ or merely $\dot{M}_{0i}(t)$. The spectrum $|\dot{M}_0(f)|$ of their sum $\dot{M}_0(t)$, in its high-frequency part, approximates the "target" spectrum in the rms sense. In time domain, $\dot{M}_0(t)$ gives the shape of the far-field body wave displacement signal for a ray normal to the fault. Similarly, using in convolution first and second derivatives of the finishing pulse (seen in Fig. 7d), one obtains the shapes of far-field velocity and acceleration signals, as illustrated in Fig. 8. Note that the operator that generates acceleration is near to the delta function; thus a heavy-tailed probability distribution of $\dot{M}_{0i}^{(\mathrm{PRE})}(t)$ is almost directly transformed to similar distribution of $\ddot{M}_0(t)$. The distribution of velocity amplitudes will have less enhanced tails.

The actual procedure includes a possible additional step needed to compensate for a secondary deficiency of the described procedure. When $\sigma_{\ln,t}$ is large, powerful acceleration spikes arise, all of the

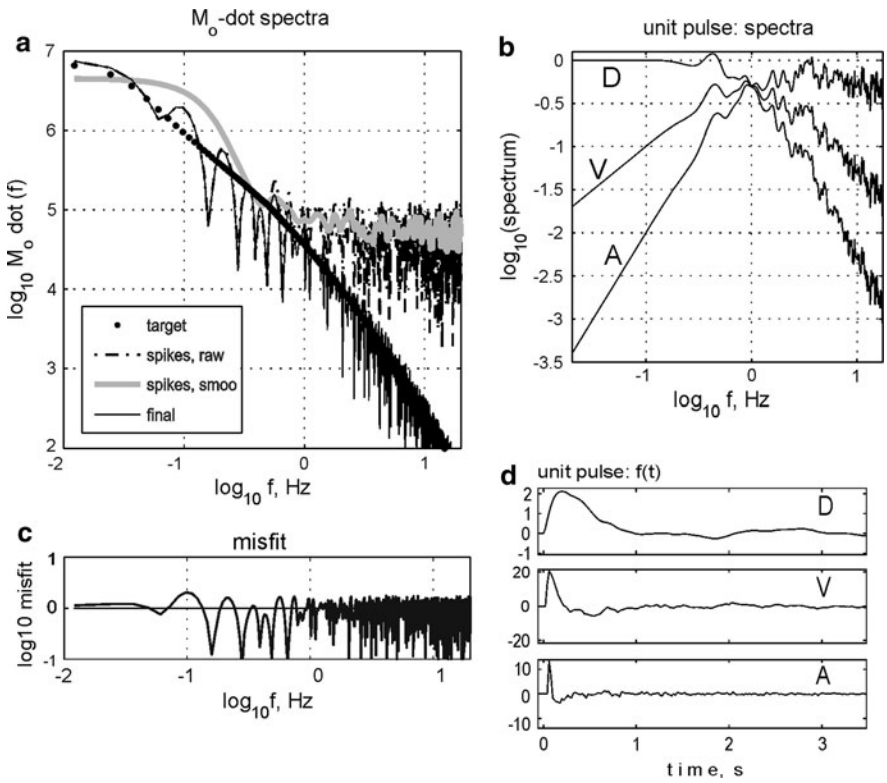

Figure 7

Modifying preliminary Fourier source spectra to match the target one. **a** Set of amplitude spectra: of the preliminary time function $|\dot{M}_0^{(\mathrm{PRE})}(f)|$ (*dashed-dot line*); its smoothed version $|\dot{M}_{0i}^{(\mathrm{PRE},sm1)}(f)|$ (*grey*), target spectrum $\dot{M}_0^{(\mathrm{TAR})}(f)$ (*dots*), and final spectrum $\dot{M}_{0i}^{(\mathrm{FIN})}(f)$ (*solid line*). **b** Amplitude spectral representation for the "finishing operator" (*D*) and its modifications; **c** spectral misfit between final spectrum and target spectrum of graph **a** ($\dot{M}_{0i}^{(\mathrm{FIN})}(f)/\dot{M}_0^{(\mathrm{TAR})}(f)$). **d** Time-domain representation of the "finishing operator," or "finishing pulse" (*D*), and its first and second derivatives (*V*, *A*); see graph **b** for corresponding amplitude spectra

same sign, producing an asymmetrically looking accelerogram that looks undesirable from the engineer's viewpoint (conversely, it may and seemingly does hint at a real geophysical phenomenon, but this topic is out of the scope of this study). A dedicated routine is designed that permits randomization of the signs of the pulses by modifying their phase spectrum. This routine introduces only minor disturbances in the timing and shapes of subsource signals; it can be enabled as needed.

The described source simulation algorithm is capable of producing realistic-looking far-field and near-field ground motions. Also, it successfully emulates, in terms of amplitude levels, observed peak accelerations and velocities, as well as response spectra and characteristic durations. However, the described procedure operates, in a certain sense, too well: its repeated runs generate signals whose amplitudes and response spectral levels vary only slightly from run to run. The cause is the feedback loop built into the described procedure for spectrum simulation, which effectively dampens the natural variability of signals. Close reproduction of target spectral shape might be acceptable for a special case when a single example trace is needed, but in general this behavior is evidently undesirable; the most unpleasant result will be significant underestimation of uncertainty of the results of seismic hazard estimation. The unrealistic, too accurate spectral fit that can be seen on Fig. 7c illustrates this problem. Therefore, one should uncoupled the feedback loop to reproduce the random variability of ground motion realistically.

Towards this end, the above algorithm was modified through the use of multiple runs of the program. In a preliminary stage, changing only the random seeds and keeping all other parameters fixed, the spectral finishing operator $U(f)$ is calculated in many (e.g., 25) runs. The results are averaged and then

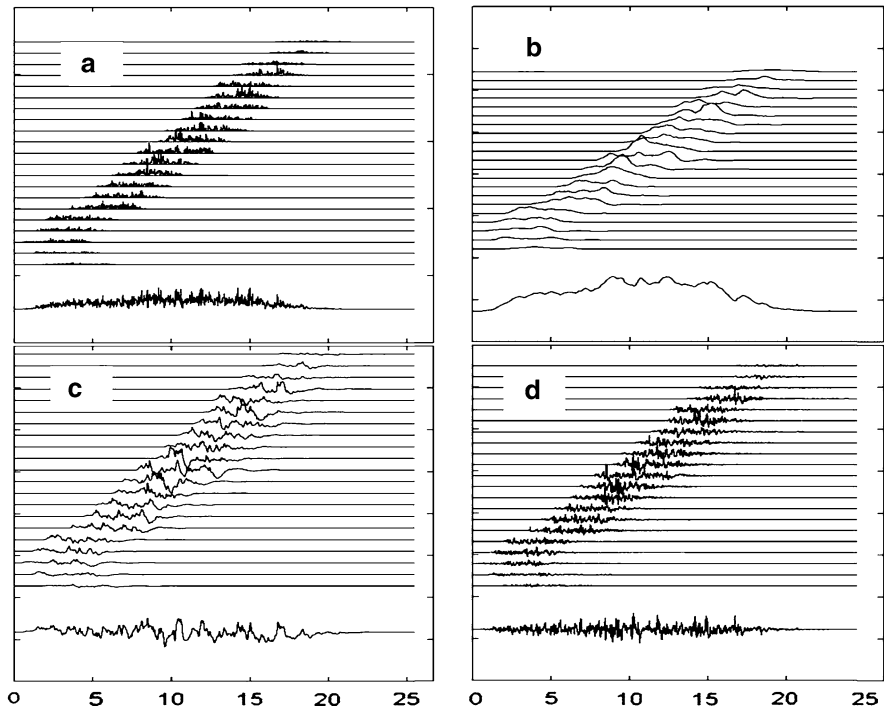

Figure 8
Example preliminary and final time functions; for improved legibility, the simplified case of a linear source (with 21 × 1 subsource grid) is given. **a** the set of $\dot{M}_{0i}^{(\mathrm{PRE})}(t)$ and the summary time function $\dot{M}_{0}^{(\mathrm{PRE})}(t)$ below; **b**, **c**, and **d** similar plots for $\dot{M}_{0i}(t)$, $\ddot{M}_{0i}(t)$, and $\dddot{M}_{0i}(t)$. Note that vertical scales for **a** and **b** differ

considered as a "mean" finishing operator. Afterwards, the simulation(s) proper is performed, with the feedback loop turned off, and the "frozen" finishing operator is used instead of an adjustable one. After such modification, the algorithm generates signals with realistic variability of parameters. Only this mode is adequate for uses such as: generating suites of design earthquake ground motion, studying its sensitivity to variations of input parameters of the model, and/or analyzing variability/uncertainty of the results.

3.10. List of Parameters of the Model

To make the described components easier to grasp, a list is given below of the most important parameters that define a single realization of our numerical model. Particular values of parameters can be selected and modified in order to: (1) tune the source model to a particular seismological situation, and (2) analyze the variability of the predicted motion and its sensitivity to parameter variations.

1. General.
   - 1.1 Moment magnitude $M_{w\cdot}$; stress drop parameter δ, defined as logarithmic deviation of the individual stress drop value from its regional average [$\delta = \log(\Delta\sigma/\Delta\sigma_{\mathrm{ref}})$].
   - 1.2 Length L and width W of the fault rectangle; numbers of subsources: n_x along L and n_y along W; subsource sizes d_x and d_y, reference subsource size $d_{\mathrm{sub}} = (d_x d_y)^{0.5}$.
2. Kinematics and dynamics.
   - 2.1 Root-mean-square deviation of logarithms of local slip $\sigma_{\ln,xy}$: defines how prominent slip asperities are in the simulated final slip function.
   - 2.2 The exponent γ in the power law that defines the 2D power spectrum ($\propto k^{-\gamma}$) of the final slip.
   - 2.3 Parameters setting the particular variant of "cap" function that defines mean shape of 2D final slip function.

2.4 Location of the nucleation point x_{nuc}, y_{nuc} along L and W.
2.5 Rupture velocity parameters: fault-average value of Mach ($v_{\mathrm{rup0}} = \mathrm{Mach}{\cdot}c_S$); relative range D_v of random perturbation of local value of rupture velocity over the fault area.
2.6 C_H parameter: rise time $T_{\mathrm{rise}} = C_H{\cdot}(L/v_{\mathrm{rup0}})$.
2.7 Root-mean-square deviation of logarithms of time function amplitudes $\sigma_{\ln,t}$: defines the degree of non-Gaussian behavior ("spikiness") of accelerograms.
2.8 A code to select a particular variant of the envelope or mean shape of local slip rate time function.

3. Random seeds and other parameters that define a particular realization of random functions (sample functions).

3.1 The random seed defining the realization of final slip function.
3.2 The random seed defining the realization of the time histories of subsources.
3.3 The random seed defining the realization of the random history of rupture velocity.

4. Random seeds and other parameters that control generation of random variants of the source (not needed for generation of a single example source; used for generation of suites of accelerograms and/or uncertainty analysis).

4.1 The random seed to fix a variant of the nucleation point position, and the values of ranges along x and y, which define intervals of its perturbation.
4.2 The random seed to fix a variant of the fault-average value of Mach number, and the value of range that defines the interval of perturbation of its value with respect to a fixed reference value (as set in 2.5).
4.3 Random seeds to fix variants for parameters δ, δ_{HF}, and the values of range that define the interval of perturbation for them.

5. A particular source spectrum scaling law adopted to describe source spectra in the study region, tabulated or in analytical form; or preset target spectrum. Parameters (δ_{HF} or A_0) that control the level of HF branch of the spectrum at given M_0.

In an actual simulation, only part of the listed parameters serve as the input set and should be preset, while others are either functions of this set or closely correlated to them. For instance: assume one fixes M_w, L, W, n_x, and n_y; this determines δ, d_x, d_y, and d_{sub}. Among medium parameters, the obligatory one is S-wave velocity c_S (the average value for the near-fault medium). Note that, for all parameters but M_0, default values and recommended brackets for their variation are supplied with the procedure.

3.11. Using Perturbation of Parameters to Characterize Uncertainty of Predicted Strong Motion

The assessment of uncertainty of parameters of predicted "typical" or "expected" ground motion is a very significant component of deterministic seismic hazard analysis. This uncertainty has many components that are mostly irrelevant to the present study, such as those related to identification of geological faults with potential sources, locating these sources on these faults, and ascribing them adequate M_w values, unit moment tensor, and position in space. Also, the uncertainty related to path and site geology is not discussed here. The only part of uncertainty to be discussed is that directly related to the properties of a particular earthquake fault. In abstract terms, these components of uncertainty can be divided into natural variability of earthquakes ("aleatoric component") and effects of our ignorance ("epistemic component"), but in practice these factors intermix. To analyze uncertainty in the scope of the presented technique of simulation, a number of approaches were tested.

There is random variability related to intrinsically stochastic part of the model. It can be analyzed jointly or separately, factor by factor, by using a series of sets of random seeds defining the final slip distribution, rupture front propagation, and local time histories of slip rate. Another kind of variability (treated as random) is related to the indeterminacy of input parameters, either natural or related to our

insufficient knowledge. Two approaches were tried in this case. The first is to randomize these parameters and to analyze variations in the same manner as in the "intrinsically stochastic" case described above. In this way, effects of variations in nucleation point position, fault-average rupture velocity, and stress drop can be and were analyzed. Another approach is to analyze the effect of systematic variation of parameter values on signal parameters. When this dependence is not very nonlinear, it can be linearized, and sensitivities can be found. With sensitivities at hand, relative contributions of input parameters to joint uncertainty can be estimated with convenience. However, this approach should be used only with great caution because both the interaction between parameters and nonlinearity of the relationships in use can easily make the results of linearized factor-by-factor analysis significantly biased. More efficient approaches are possible, in particular those that permit analysis of interaction between factors; methods of design of experiment may be of value.

The analysis of variability may greatly help in understanding relative contributions of different factors to the general uncertainty. This knowledge is crucial for judging the validity of predicted strong motions. Also, only this kind of analysis permits one to generate meaningful suites of "representative variants" of possible ground motions. Indeed, if one has not identified the main components of uncertainty and their relative weights, one cannot form a clear idea of which deviations of input parameters from their initial reference values may produce significant hypothetic "anomalies" of future event. From a seismologist's viewpoint, this kind of analysis may form a sound basis for constructing adequate suites of accelerograms for engineering analysis.

4. *Examples of Application of the Proposed Procedure and Dedicated Program Codes*

4.1. *Strong Motion Simulator: Procedures and the ACCSYN Program Package*

Having constructed the finite source model by the above-described procedure, in a practical application one has to pass to the calculation of strong motions proper. If one confines himself to the case of sites where nonlinearity of the medium can be ignored (rock and in many cases stiff soil), the calculation of strong motion can be based, as usually, on combination of subsource time histories with appropriate Green functions. It should be mentioned that, in the current version of the simulation procedure, subsource strike, dip, and slip are fixed and identical for all subsources, and the source is assumed to consist of a single planar rectangular rupture.

To match the level of description provided by the source simulator, a broadband Green function calculator is needed. In practice, I used an original discrete-wavenumber code based on matrix impedance method (Pavlov, 2002, 2006, 2009; Gusev and Pavlov, 2009) that calculates pulse response of layered elastic medium. For this, often realistic, case it provides an accurate broadband representation of ground motions, and has no intrinsic limitations with respect to layer thickness and bandwidth. In particular, it predicts equally well both so-called fling at zero frequency, and high-frequency body wave spikes.

The final stage of calculation is performed by the convolution module. Its first step is to convolve the subsource time histories and the corresponding subsource Green functions for a certain site over time. The second step is to add thus-obtained contributions of all subsources, resulting in the ground motion at the site. In addition, attenuation corrections [through $\exp(-\pi jf)$ factor (Anderson and Hough, 1984) and distance-dependent term] are added here. Alternatively, frequency-independent Q profile can be included in the main procedure for Green function calculation.

The sequence of PULSYN code, GF calculator, and convolve-and-sum module is organized as the program package called ACCSYN.

In the following, examples of application of the ACCSYN package are given in condensed form to illustrate the presented approach; the reader is addressed to original publications for more details. Entire work with applications was performed in close cooperation with V.M. Pavlov, who provided the Green function calculator code and supported its use. Of the three cases presented, in the first two the main aim was to test and validate the general approach, and ACCSYN was used to emulate the observed strong

motions realistically. In the third case, an attempt was made to simulate unknown strong motion.

It is necessary to mention that the success of fitting real data by the results of simulation is understood here in the engineering seismology sense. For both LF and HF signals (displacements and accelerations), judgment (informal) was based on the likeness of the general appearance, and on the acceptable fit of duration, peak amplitudes, response spectra, and smoothed amplitude Fourier spectra.

4.2. Northridge 1994 Earthquake: Near-Source Simulation and Analysis of Uncertainty

General issues. The algorithm described above was applied for emulation of a series of 19 near-source accelerograms obtained in the epicentral zone of the $M = 6.7$, 1994, Northridge, California, earthquake on various ground types (GUSEV and PAVLOV, 2009); see the preprint (GUSEV and PAVLOV, 2006) for a more detailed version, especially as regards uncertainty analysis. Parameters of the model were set on the basis of published data; the only parameter whose values were fit to real data is the κ (kappa) parameter. According to stratigraphy, stations were divided into three groups: "rock," "deep soil," and "intermediate," each group with its own vertical profile. See Fig. 9 for a general overview of the fault and stations. A commented list of assumed values of main parameters follows:

Fault center: $\varphi = 34.28°$; $\lambda = -118.56°$; $H_c =$ 12.5 km; strike = 122°; dip = 40°; rake = 101°;
Nucleation point: $\varphi = 34.35°$; $\lambda = -118.54°$; depth = 17 km (as obtained in inversions); $M_w =$ 6.7; $L = 18$ km; $W = 24$ km;
$v_{\text{rup0}} = 3$ km/s (Mach = 0.85), $T_{\text{rise}} = 0.7$ s ($C_H =$ 0.1); subsource grid 7 × 7; $DV = 0.8$; $\gamma = 1.5$;
$\sigma_{\ln,t} = 0.5$ (a tentative value);
$\sigma_{\ln,xy} = 0.5$ [A tentative trade-off value between cases of slightly perturbed, nearly constant slip ($\text{CV}_{xy} < 0.3$) and very expressed "asperities" ($\text{CV}_{xy} > 1$); at present appears too low].

Scaling law of source spectra: for the particular case of Western USA, Brune's ω^{-2} law, in the version of JOYNER (1984), with reference stress drop value of 50 bar, is treated as the regional average.

Stress drop: set at 75 bar (as published) or 1.5 times the assumed regional average ($\delta = 0.18$).

The example simulations shown below are selected from ten runs of the simulation procedure, changing the three random seeds (see paragraph 3.10 above, subsections 3.1–3.3); they show ground motion parameters quite near to observed ones. The ranges of variations of these parameters were analyzed separately, as will be shown further. See Fig. 9 for example subsource time functions. Based on Fig. 10 one can compare simulated and observed time histories of ground motion at five representative stations. The differences between simulated and

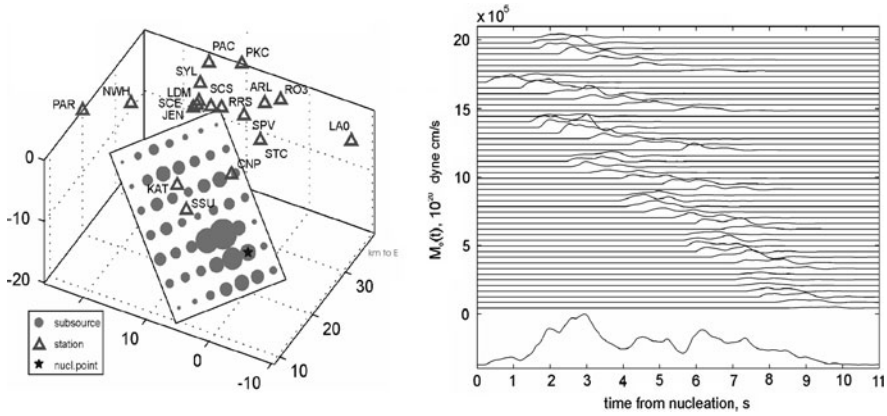

Figure 9
Left perspective view of the fault rectangle and receivers/stations for the $M_w = 6.7$, Northridge, 1994 event. The subsources are indicated as *dots*; their sizes reflect the value of subsource seismic moment in a particular simulation run. *Star* is the nucleation point. Coordinates in km. *Right* moment rates $\dot{M}_{0i}(t)$ for 49 subsources of this run and their sum

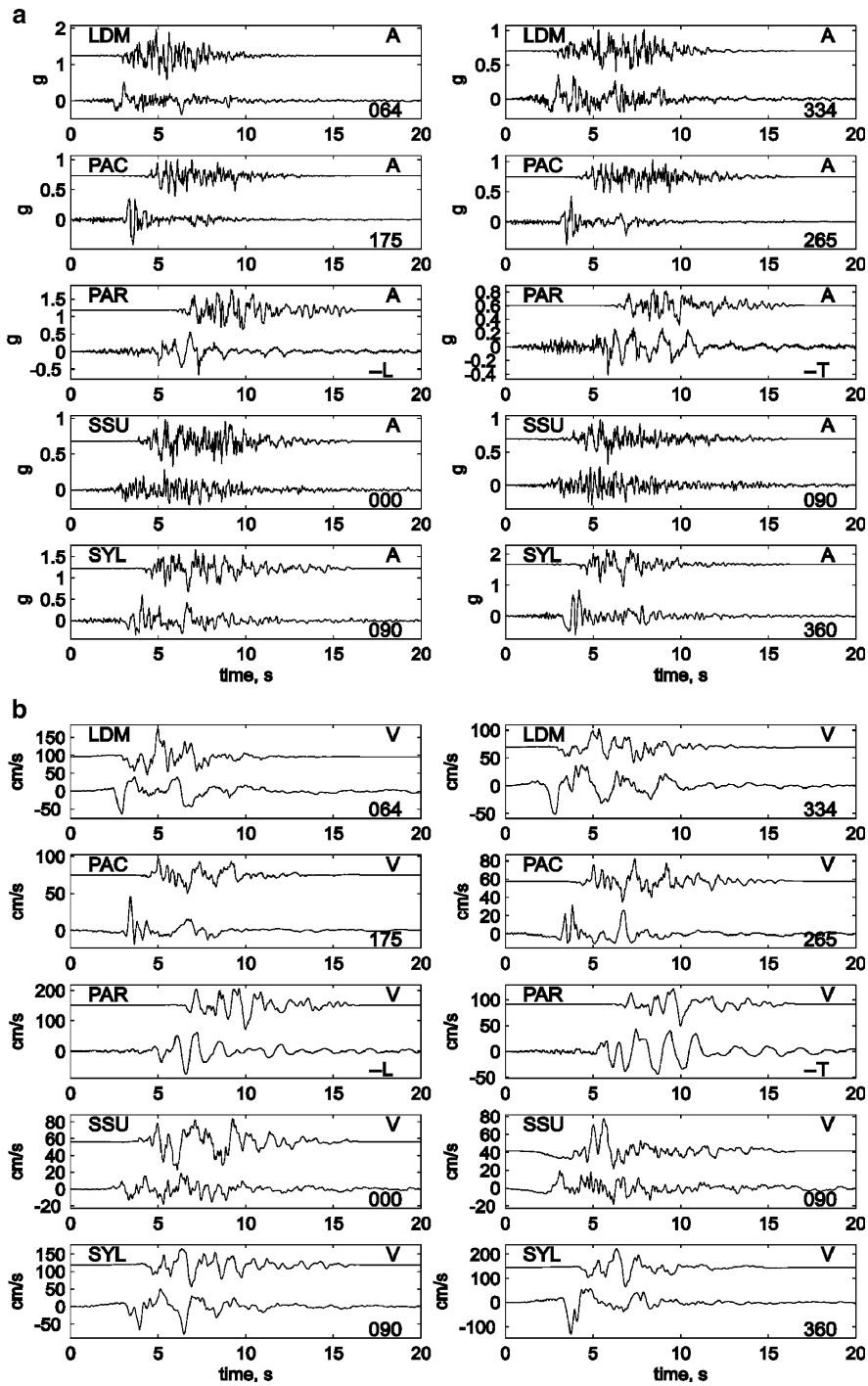

Figure 10

Comparison of observed and simulated (for the preferred run) time histories for acceleration (**a**), velocity (**b**), and displacement (**c**) for five stations, for two horizontal components. In each box, the lower trace is the observed one and the upper trace is the simulated one. Ground types are: rock for PAC and LDM, soft rock for SSU, and deep soil/basin for PAR and SYL. Note that simulated acceleration traces for rock stations are less spiky than observed ones; this seemingly indicates that the selected value of $\sigma_{\ln,f}$ is too low

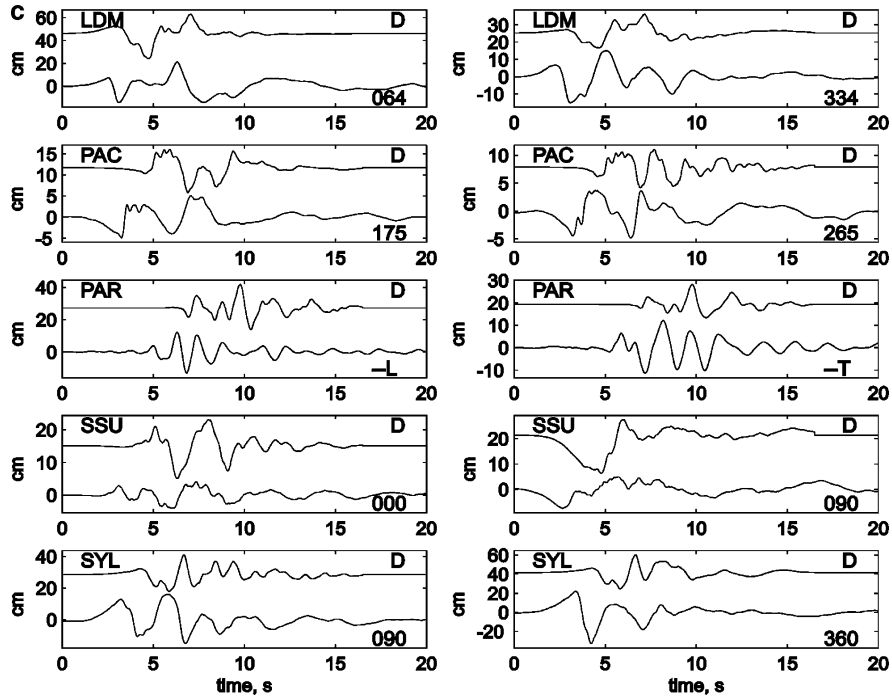

Figure 10
continued

observed time functions were analyzed in the form of logarithmic amplitude misfit, denoted generally as $\Delta\log(A) = \log_{10}(A_{\text{simulated}}) - \log_{10}(A_{\text{observed}})$. Misfit was determined for pseudo response acceleration PRA [$\Delta\log_{10}$(PRA)] calculated over 25 frequencies covering the 0.1–20 Hz range with an approximately constant step in log frequency; and also for peak amplitudes of acceleration, velocity, and displacement, and averaged over 19 stations (Fig. 11). The particular misfit of PRA around 0.2–0.5 Hz noticeable on the left plot is a property of the individual sample source and is greatly reduced for another sample source as seen in the adjacent plot. Such misfits represent natural variability of spectra for sources simulated with identical sets of parameters and different random seeds.

Uncertainty analysis. The uncertainty characteristics of the simulated ground motion for the 1994

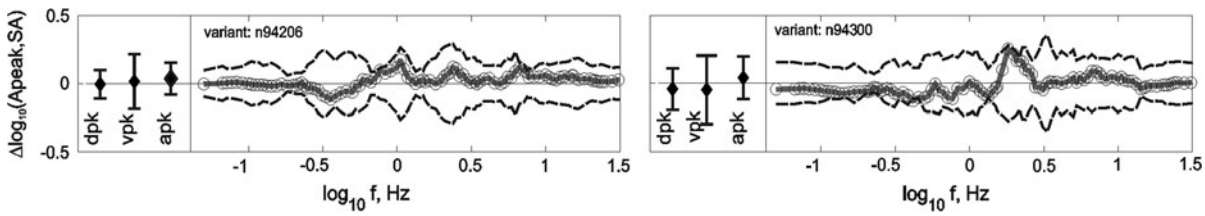

Figure 11
Misfit of horizontal peak amplitudes and acceleration response spectra PRA(*f*), for two simulation runs for the Northridge 1994 event. Average values over two horizontal components are given. The misfit values are the differences (simulated minus observed) between $\log_{10}$ peak displacements *D*, velocities *V*, and accelerations *A* (*left box* in each graph), and for $\log_{10}$ pseudo response accelerations (right box). See Table 1 for the components of scatter of misfit of peak amplitudes, $\Delta\log_{10}(A)$ and $\Delta\log_{10}(V)$. Average misfits and their standard deviations over 19 stations for the same data are shown, as *diamonds* with *error bars* for amplitudes, and as *line* with *circles*, and a corridor around zero level for spectra. Both rms scatter and systematic shifts vary from one simulated sample source variant (on the *left*) to another (on the *right*) because they include significant random element; two plots for two variants illustrate these variations

Northridge earthquake were analyzed along the lines given in the corresponding section above. The uncertainty component relating to fault properties was estimated, among other components, by perturbing, randomly or systematically, many fault-related factors. In this analysis, average values of $\Delta\log_{10}(A)$ over 19 stations were analyzed. The scatter of these averages from one simulation run to another permits the measurement of uncertainty related to a particular perturbed factor. As a byproduct of such analysis, interstation scatter was also determined in each run (and averaged over runs), yielding a reference for comparing source-related and site-related components of uncertainty. Three contributions of the purely stochastic part of variability were examined in the following manner. In the first series of variants, ten different random seeds were used that defined ten particular versions of the final slip field, whereas the random seeds defining rupture history and subsource time histories were fixed. In the second run, in similar manner, ten seeds defined ten realizations of random rupture history, whereas slip and time histories did not change. Similar testing was performed to estimate the component of variability related to randomness of the set of time histories. Then, the effects of unknown fault-average rupture velocity value (Mach taken as uniform random in the range 0.6–0.9), and nucleation point position (anywhere in the lowermost one-third of the rupture surface) were studied by randomly perturbing these parameters (but keeping the three former random seeds fixed). For other analyzed factors, the sensitivity approach was applied, where sensitivity is defined as the derivative dy/dx where x is an input parameter and y is a ground motion parameter. First, the value of sensitivity for a parameter perturbation was estimated by numerical tests; then it was combined with the a priori value of rms scatter of this parameter to result in the expected rms scatter of $\Delta\log_{10}(A)$. The determined sensitivity estimates were relatively reliable, whereas the assumptions regarding the scatter of input parameters were mostly guesswork. These guesses (Table 1)

Table 1

Uncertainty analysis for predicted acceleration (A) and velocity (V) peaks for the Northridge 1994 case (averages of peaks over two horizontal components)

No.[a]	Factor/parameter	$\sigma(p)$[b]	Sensitivity $d[\log(A)]/dp$	Sensitivity $d[\log(V)]/dp$	$\sigma_{\log}(A)$[c]	$\sigma_{\log}(V)$[c]
1	$D(x, y)$	–	–	–	0.054	0.051
2	$\dot{M}_{0i}(t)$	–	–	–	0.026	0.042
3	$v_{\text{rup}}(t)$	–	–	–	0.047	0.064
Σ *stochastic*					0.076[d]	0.092[d]
4	Mach	–	–	–	0.052	0.079
5	x_{nuc}, y_{nuc}	–	–	–	0.027	0.048
6	log $\Delta\sigma$ or δ	0.1	0.31	0.42	0.031	0.041
7	$\sigma_{\ln,t}$	0.15	0.24	0.18	0.035	0.027
8	$\sigma_{\ln,xy}$	0.15	0.06	0.10	0.009	0.015
9	H_c	2.5 km	0.023	0.021	0.057	0.053
10	Dip	10°	0.0015	0.0033	0.015	0.033
11	log M_0	0.1	0.3	0.4	0.03	0.04
Σ *source*					0.11[e]	0.13[e]
12	Site	–	–	–	0.14[f]	0.13[f]
Σ *total*					0.18[g]	0.18[g]

By p, an arbitrary factor (any among numbers 4–11) is denoted. All logarithms are decimal

[a] The number of a factor or of a parameter; unnumbered rows give standard deviations for combined effects, assuming independence of factors

[b] Standard deviation of a factor, assumed tentative value (a guess)

[c] Standard deviation of $\log_{10}$ peak amplitude on horizontal component, average over two components

[d] Combined over factors 1–3

[e] Combined over factors 1–11

[f] An empirical estimate derived from interstation variance

[g] Combined over contributions of the "source" and "site" rows

were rather moderate, not "conservative." Thus, the entire analysis should be treated as an exercise, although still realistic. The uncertainty analysis was performed with respect to peak amplitudes and response spectra at 18 periods, all for averages over two horizontal components. Part of the results is given as Table 1. It includes eight inner source factors and parameters, with fault center depth, rake, and M_0 value added. Also, the site component of amplitude scatter (empirical estimate) is given for reference. The average interstation misfit of 0.14 (row 12 of Table 1) represents the uncontrolled uncertainty related to deviations of actual path/geology effects at individual sites and paths from the values defined by the modeled Green functions. Initially, two more fault parameters were analyzed: γ and D_v, but their effects happened to be small and the values of corresponding sensitivities were uncertain.

Analysis of Table 1 and other data indicated the following. Contributions of each of three purely stochastic factors are of the same order of magnitude. The largest contribution is from the stochastic variability of the final slip map. The smallest contribution is from subsource moment rate time histories. This may seem counterintuitive but agrees with the known fact of relative stability of extremal values of a random function. The effect of stochastic variability of details of rupture propagation history is intermediate among the three. Other stochastically treated factors include the most significant individual factor; i.e., the fault-average value of rupture velocity or Mach, acting probably through signal duration. The contribution of variations of the nucleation point position is limited. Generally, the effect of this factor, which defines directivity effects, might be much larger. The obtained figure is at the lowermost end of its real range, because the receivers are on the free surface, and the nucleation point is confined within the deeper part of the dip-slip fault. In this special case, the directivity effect is similar or comparable for most stations. The subsequent parameters were analyzed through the sensitivity approach; the results regarding these factors are less convincing, because they are based on the tentative assumed values for the rms deviations of input parameters. The effect of log $\Delta\sigma$ (i.e., δ) is moderate. Note that it is analyzed keeping the value of M_0 fixed, and is related to the combined effect of two intermediate factors: the increase of HF spectral level, and, less evidently, the decrease of fault size and therefore of signal duration. The effect of $\sigma_{\ln,t}$ is moderate but quite noticeable, as can be expected, as this factor directly modifies the peak factor (peak-to-rms amplitude ratio) of the signal. The effect of $\sigma_{\ln,xy}$ (as well as of the exponent γ of wavenumber spectrum) is small; this is unexpected and deserves further attention. The effects of H_c and of dip are given for illustration only; they depend on the actual fault–station geometry and cannot be generalized at all. Stochastic and parameter-related uncertainty jointly resulted in source-related rms uncertainty of 0.11 for log(A). Also, for illustration, I cite the empirical estimate of intersite scatter based on the misfit of predicted amplitudes to the observed ones. One can see that, despite separation of stations into three groups, a significant part of propagation and site effects is still unexplained and manifested as intersite scatter, comparable to the estimated effect of fault-related factors. Site-related rms uncertainty of 0.14 and source–related rms uncertainty of 0.11 are combined to result in total uncertainty of 0.18.

Each summary fault-related effect shown in Table 1 (or Fig. 11) estimated for averages over two components should be multiplied by 1.1–1.4 to make a figure that characterizes the maximum horizontal amplitude. Therefore this parameter may be characterized by the value of the fault-related rms uncertainty of about 0.14–0.17 $\log_{10}$ (or 0.32–0.39 $\log_e$) units. This value can be treated as a reasonable minimum characteristic; numerically it looks satisfactory and suggests that our simulation procedure can be considered as consistent. In addition, durations and general appearance of simulated records reasonably match those of observed ones. Bazurro *et al.* (2004) analyzed how well the results of the described simulation, and also of six other techniques for simulation of ground motion can emulate peaks of linear and especially nonlinear response of single-degree-of-freedom system to the observed motion. Among seven simulated data sets, the technique described above was the only one that produced acceptable results over the wide (0.25–10 Hz) frequency range analyzed.

4.3. Intermediate-Depth 24 November 1971 Kamchatka Earthquake

The large earthquake of 24/11/1972 with hypocenter near Petropavlovsk-Kamchatsky ($M_w = 7.6$, $H_c = 105$ km, epicentral intensity $I_0 = 7$–8 MSK, Fig. 12a), was recorded on horizontal components of strong motion velocimeter ISO-S5S at the seismic station "Petropavlovsk" (PET). This is the largest-amplitude strong motion record obtained in Petropavlovsk-Kamchatsky, and its simulation provides a possibility to test the developed technique for the case of a subduction earthquake (Gusev *et al.,* 2009). On the basis of earlier studies it was possible to define geometric parameters and duration of the rupture. The fault plane is near-vertical, and rupture process is nearly bilateral. See the main source parameters in the list below, and the subsource grid on Fig. 12b. Large rupture duration combined with bilateral rupture mode suggests rather low average rupture velocity. Of the overall source parameters, two—fault rake and M_w—were adjusted during the simulation; also, two spectral parameters were fitted. The entire search was of trial and error kind. In addition, a considerable amount of trial and error was needed before this search to establish an appropriate analytic form for the description of spectral shape. As a final result of fault parameter selection, the following features of strong motion were simulated successfully: peak acceleration, velocity, and displacement (Fig. 13); strong motion duration, Fourier spectrum (Fig. 14), and response spectrum. A peculiarity of the 24/11/1972 event is its rather high level of HF acceleration spectrum, probably related to interslab position of the rupture.

Here is the list of assumed values of main parameters:

Fault center: $\varphi = 52.79°$; $\lambda = 159.59°$; $H_c = 105$ km; *nucleation point:* $\varphi = 52.71°$; $\lambda = 159.47°$; depth 105 km;
Strike = 43°; dip = 83°; rake = 85–110° (published, from three sources) adjusted value 120°;
$M_w = 7.1$–7.7 (published, from four sources), adjusted value 7.65; $L = 70$ km; $W = 60$ km; subsource grid 11 × 9;
$v_{\text{rup0}} = 1.1$ km/s (Mach = 0.28), $T_{\text{rise}} = 5$ s ($C_H = 0.1$); $DV = 1.5$; $\gamma = 1.0$; $\sigma_{\ln,t} = 0.75$; $\sigma_{\ln,xy} = 1$; $\kappa = 0.055$ s.

To fit the observed spectral shape, the Atkinson (1993) 2-Brune formula was used,

$$\dot{M}_0(f) = M_0\left(\frac{1-\varepsilon}{1+(f/f_a)^2} + \frac{\varepsilon}{1+(f/f_b)^2}\right), \qquad (17)$$

with lower f_a and upper f_b corner frequencies and the ε parameter that determines details of spectral shape. Let us introduce two HF acceleration spectral levels:

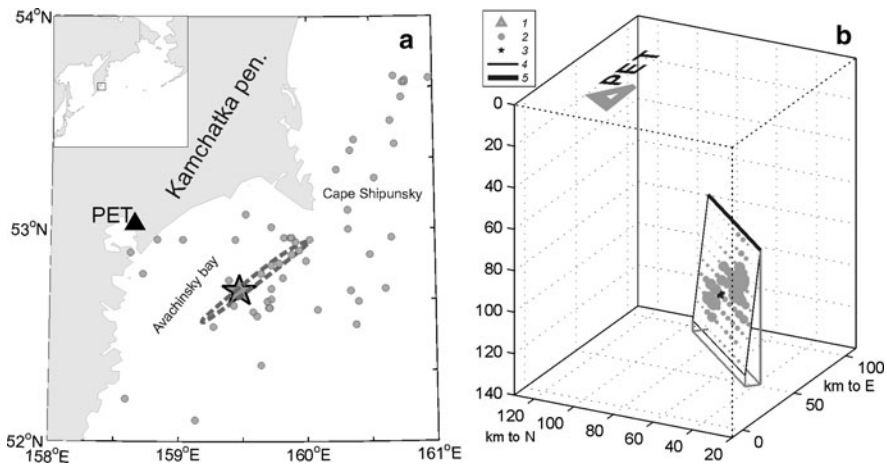

Figure 12
Study area and source model geometry for the 24/11/1971 Kamchatka event. **a** Map, star is the epicenter, and *grey dash* ellipse is fault surface (with nearly vertical dip) deduced from aftershocks and other data; **b** perspective view of the fault model: *1* station, *2* subsource, *3* nucleation point, *4*, *5* fault surface edges, *5* the upper edge. Subsource symbol size reflects its seismic moment value

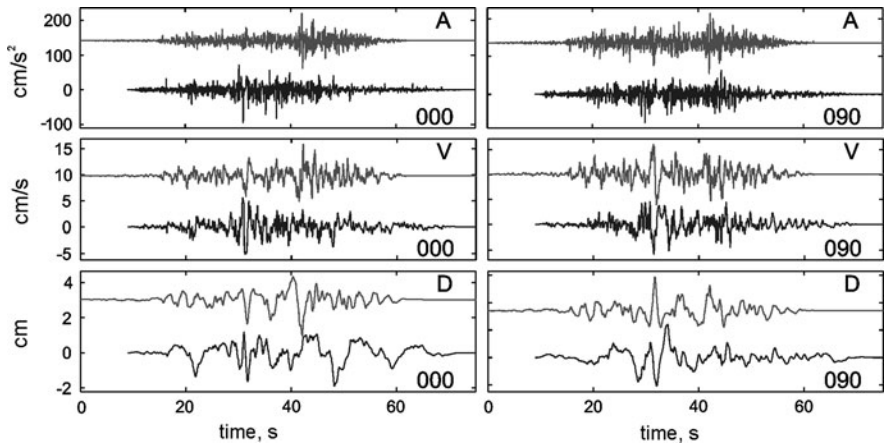

Figure 13
A variant of simulated ground motion (*upper* in each box) compared with the observed one (*lower* in a box). Relative time shift selected by eye. Both kinds of data were passed through a high-pass filter with 0.07 Hz cutoff. *Top to bottom* acceleration, velocity, and displacement; *left* NS component, *right* EW component. Unfiltered simulated displacements included static offset of −2 cm (*NS*) and +3.5 cm (*EW*)

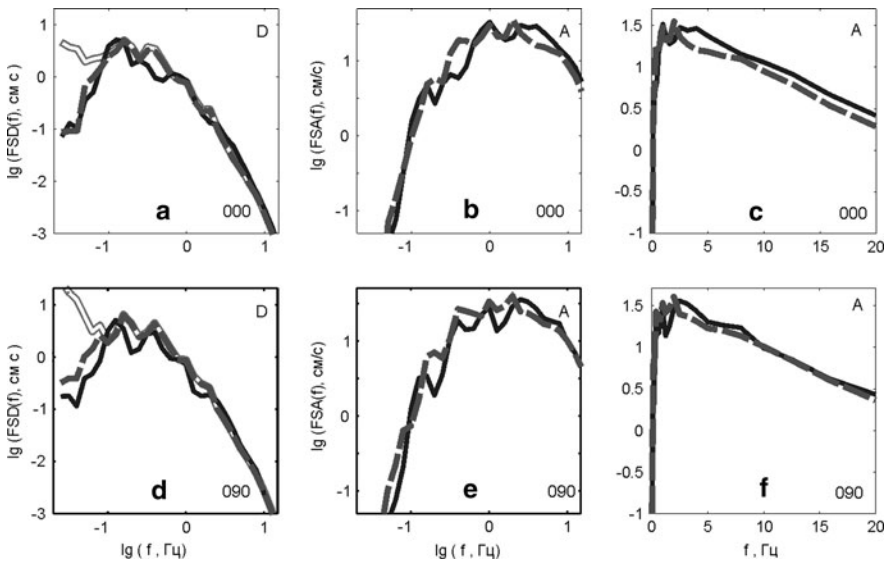

Figure 14
Amplitude Fourier spectra for simulated displacement (**a**, **d**) and acceleration (**b**, **c**, **e**, **f**) traces of Fig. 13 (*dashes* for filtered traces; *double grey* for original unfiltered traces) as compared with similar spectra of observed traces (*solid*). *Top row* NS, *bottom row* EW. Scale is log–log for **a**, **b**, **d**, and **e**; for **c** and **f**, the frequency scale is natural, to illustrate the appropriate choice of the spectral decay parameter κ that reflects mostly path attenuation effect. Spectra were smoothed using a 0.1 decade window

true HF acceleration spectrum level AHF, and similar eventual level defined by the corner anchored at f_a (when $f_a = f_b$, $A_0 = A_{\mathrm{LF}}$). It is easy to see that $A_{\mathrm{LF}} = M_0(2\pi f_a)^2$, and that $\varepsilon = (A_0/A_{\mathrm{LF}} - 1)\Big/\left((f_b/f_a)^2 - 1\right)$. Our estimate for f_a is based on the $f_c(M_0)$ trend of the semi-empirical spectral scaling law of Gusev (1983), which can be written as

$$\begin{aligned}\log f_c &= 7.6 - \log_{10} M_0/3 + \delta/3 \\ &= 2.25 - 0.5M_w + \delta/3,\end{aligned} \tag{18}$$

where the term $\delta/3$ represents possible correction for a nonstandard value of stress drop. The value for δ was assumed to be the standard one: $\delta = 0$, making $f_a = f_c = 0.0266$ Hz. The initial estimate for A_0 was taken from the empirical trend for Japan after Dan

et al. (2001), verified by IRIKURA (2007). Adding the correction term δA_{HF} to account for nonstandard A_{HF}, their result is:

$$\begin{aligned}\log A_0 &= 17.391 + \log M_0/3 + \delta A_{\mathrm{HF}} \\ &= 22.741 + 0.5M_w + \delta A_{\mathrm{HF}}. \end{aligned} \quad (19)$$

The values of two correction parameters $\delta A_{\mathrm{HF}} = 0.76$ and $f_b = 0.56$ Hz were found by trial and error. The sign and amount of deviation of A_{HF} from the average Japanese trend is in good agreement with the position of rupture in the mantle and its intraslab character, representing a tear in the oceanic plate.

4.4. A Hypothetic Messina Straits Earthquake

In relation to the plans (suspended at present) to build a bridge connecting Sicily to mainland Italy over Messina Straits, it was interesting to estimate possible longer-period ($T > 1$–2 s) components of the ground motion at its piers. This attempt is described in (GUSEV *et al.*, 2008). As a scenario event, a repetition of the devastating 1908 Messina earthquake ($M = 7$) was taken, with reverse dip-slip causative fault located just under the straits (Fig. 15a). As the shortest fault-to-site distance is only 3–5 km, the kinematic earthquake rupture process has to be described in sufficient detail. To represent the 40 × 20 km fault, a dense 33 × 15-element grid of subfaults was used (Fig. 15b). The horizontal upper edge of the rectangle is at 3-km depth, and the upper northern corner of the rectangle is under the piers. Thus, the condition was fulfilled that the shortest fault-to-site distance (3–3.5 km) must be significantly larger than subfault size (1.33 × 1.25 km). Here is the commented list of assumed values of main parameters:

Fault center: $\varphi = 38.09°$; $\lambda = 15.61°$; $H_c = 7.85$ km; (upper edge depth = 3 km); strike = 20°; dip = 29°; rake = 270°;
Nucleation point: $\varphi = 37.94°$; $\lambda = 15.53°$; depth = 7.85 km; $M_w = 7.0$; $L = 40$ km; $W = 20$ km;
$v_{\mathrm{rup0}} = 2.55$ km/s (Mach = 0.75); $T_{rise} = 2$ s ($C_H = 0.1$); subsource grid 33 × 15; $DV = 1.2$; $\gamma = 1.8$; $\sigma_{\ln,t} = 0.5$; $\sigma_{\ln,xy} = 1.0$.

Scaling law of source spectra: according to GUSEV (1983), $\delta = -0.05$ [output, not preset value, defined from the requirement to make the set (M_0, L, W, and $\Delta\sigma$) compatible], $\delta_{\mathrm{HF}} = 0$.

For the fault nucleation point, the least favorable place is assumed, at the fault side farther from the sites. When setting parameters for simulation, inner parameters of the fault were assumed on the basis either of the published work aimed at the inversion of slip at the 1908 causative fault (VALENSISE and PANTOSTI, 1992) or from the experience with simulation of the Northridge 1994 case described above. Green functions for each subfault–pier combination were calculated for layered half-space models of stratigraphy under each pier. The obtained series of simulated motions (Fig. 16) was converted to the set of response horizontal velocity spectra (PRV).

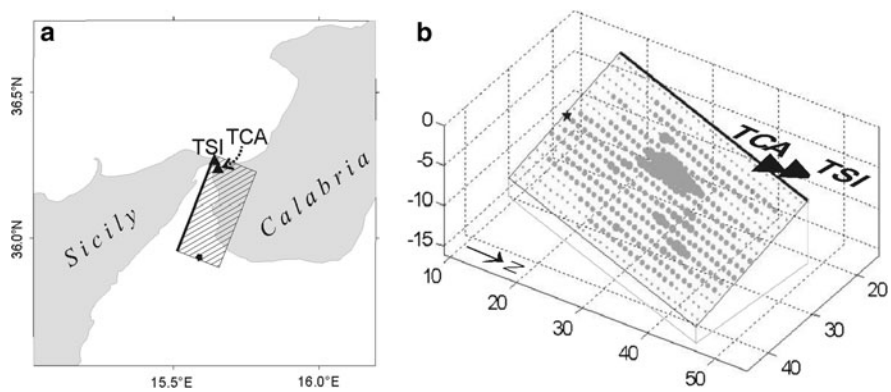

Figure 15
Study area and source model geometry for a hypothetic Messina Straits earthquake. **a** Map, hatched quadrangle is the assumed fault and the star is the assumed worst-case epicenter; planned piers/receivers are TSI ("Torre Sicilia") and TCA ("Torre Calabria"). **b** Perspective view of the fault model; each subsource is seen as a grey dot whose size reflects its seismic moment value

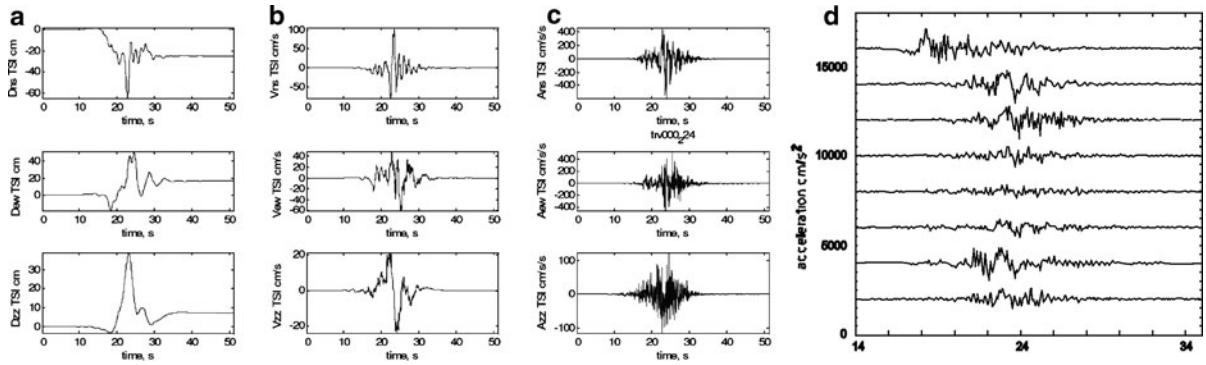

Figure 16
Simulated traces. **a**, **b**, **c** Columns of boxes contain: displacement (**a**), velocity (**b**), and acceleration (**c**) for the site TSI and variant 222; rows, *top to bottom*, show components NS, EW, and *Z*. **d** Nine variants of NS acceleration traces at TSI

Median and rms deviation of $\log_{10}$PRV for the simulated series of possible ground motions were compared with the "reference" PRV that was previously considered as a reasonable upper bound for ground motion near the piers ["Stretto di Messina, Approfondimenti relativi al terremoto di progetto per l'opera di attraversamento", Rapporto tecnico, Ref. DT/ISP/S/E/R1/001 (2004)]. Our results suggest that the seismic ground motion under the northern ("Torre Sicilia") pier dominates over that under the southern ("Torre Calabria") pier. Our median ($\approx$mean log) PRV estimate is generally above the reference one, about 1.1–1.3 times for $T > 4$ s, and up to two times for 1 s $< T \leq 4$ s. At periods longer than 10 s, our median prediction differs only slightly from the reference one. The use of advanced fault and medium models, which take into account also the natural scatter of individual PRV due to individual variability among events with the same gross source parameters, may provide a sound basis for deterministic engineering estimates of future seismic ground motion.

In the series of simulations, final slip map, local slip time histories, and the time history of rupture propagation were randomly perturbed; Mach value was drawn as uniform random in the range 0.7–0.8 (probably too narrow). All other parameters were fixed. The resulting scatter of response spectra is maximal just in the range of possible pier natural periods, of 3–10 s. The estimated standard deviations of $\log_{10}$PRV for a single horizontal component are 0.22, 0.30, 0.22, and 0.20 at the periods of 2, 5, 10, and 20 s, respectively.

Several tests were made to understand how reliable the result is. First, the effect of change of the subsource size was checked. With a doubly rarefied grid (17 $\times$ 9 subsources), spectral amplitudes in the range $T = 3$–20 s changed by no more than 10%; in the range $T = 5$–20 s they were essentially identical. Thus, one can expect that, in the moderate to low frequency range, the discretization used introduced no significant error.

In another test, the spectral scaling was assumed to follow Brune's ω^{-2} law, in the version of Joyner (1984), with $\Delta\sigma$ set at 50 bar. Resulting response spectral amplitudes in the period range 2–15 s increased 1.1–1.4 times, as could be expected comparing source spectral shapes. In our opinion, this is, rather, an overestimate.

5. Discussion

The fault simulation methodology described above is intended to combine several semi-empirical generalizations regarding fault rupture formation and generation of seismic waves in a broad frequency band. The results of elastodynamic modeling of ruptures were mostly ignored. This position is not to be understood as indicating that such studies are considered irrelevant to estimates of strong motion for engineering purposes, but rather that real faults are too complex for such approaches to be efficient in their present form up to high frequencies. Despite some clear success (Beroza and Mikumo, 1996),

causes of formation of slip pulse remain undetermined, creating difficulties for reliable prediction even of low-frequency strong motion. As for the elastodynamic approach to explain HF radiation, the situation here is worse because at present there is no systematic approach to multiple-scaled rupture dynamics, and this kind of treatment seems to be inevitable if one wishes to explain, e.g., the notorious ω^{-2} spectral asymptotes that seem to be a reasonable starting approximation for description of spectral shapes. The methodology of IDE and AOCHI (2005) may be considered as a certain success, but much remains to be done. Thus, one can believe that, in the near future, the semi-empirical approach will be the main instrument for practical simulation of strong motion. It was noted in the "Introduction" that the presented simulation procedure was designed on the basis of the concept of fragmented, randomly shaped "incoherent" rupture front, as opposed to the often-assumed "coherent" propagating crack tip. Although the concept of rupture front incoherence hardly needs revision, the actual numerical scheme is phenomenological in essence, and might incorporate other conceptual variants of rupture front. However, the variant of widely and frequently oscillating value of instant crack tip velocity that does not change sign is probably unrealistic (DAY *et al.*, 2008).

The claim that the present procedure is able to simulate fine details of fault motion and therefore can help to simulate ground motion for arbitrary small fault-to-receiver distance should not be taken as a strong assertion. The credibility of such simulations cannot be very high, because at present only some reasonable guesses [based on models such as those of ANDREWS (1981)] can be proposed to describe the spatial correlation structure of the source at small scales; also the question of local variation of rise time is poorly understood. Still, the proposed approach seems to have advantages over those based upon composite-crack finite-fault models.

One can note that the list of parameters that are needed in the described approach to specify a fault may look rather long. In my opinion, in constructing a realistic or a "bad case" simulated source, there is no way to make this list much shorter (on the contrary, this list may well need expansion). A partial solution to this difficulty is systematic specification of default values and, in many cases, typical bounds for parameters that happen to be poorly known. It should be understood that specification of a realistic scenario earthquake is not a simple procedure. Nature does not behave primitively here. On the other hand, not all parameters may be relevant for a particular project. For instance, a large-size construction, with its natural period of, say, 3 s, is not susceptible to acceleration spikes, but setting a plausible spectral shape at intermediate frequencies is a must.

Some progress can be expected if one incorporates more systematically fractal and multifractal descriptions of earthquake processes. The random final slip function used in this paper, with power-law power spectrum and lognormal distribution of values, is essentially a multifractal and actually follows the lognormal multifractal concept [SCHMITT and MARSAN, 2001; see also the "Nonconservative_III" function in (MARSAN and BEAN, 2003)]. A similar comment applies to local slip rate time histories. In the above presentation, lognormal distributions were fitted to data in a rather rough manner; also other possibilities within the multifractal concept (e.g., log-Levy laws) have not been analyzed. One may expect that, after detailed study, significantly better description of stochastic space–time source development can be obtained along such lines. Encouraging in this respect is the recently revealed (GUSEV, 2010) approximately fractal temporal structure of instant power of teleseismic HF body wave signal.

The presented technique has not incorporated some empirical fault properties that were considered as secondary; they however definitely deserve to be included in the next version of the package. These properties include nonconstant unit tensor of subfaults. As noted by YU *et al.* (1995) and ZENG *et al.* (1995), the assumption of constant unit tensor is insufficient to explain data. Random wiggling of local strike, dip, and rake, or some equivalent modification (such as using the mean orientation of tensor combined with "effective," smoothed radiation patterns) must be added for more credible simulation. Another addition may be random or systematic variation of rise time over the fault. Similarly, the HF radiation capability, at present assumed to be uniform over entire fault that is characterized by a single value of A_0 or $\Delta\sigma$(HF), can be made position dependent.

6. Conclusions

Simulation of realistic ground motion from a scenario earthquake, with adequate brackets on the parameters of this motion, is a complicated problem. A significant part of this problem is simulation of space–time structure of an earthquake source. A new advanced technique for such simulation is presented, intended for the use in practical characterization of possible strong motion and estimation of its uncertainty. The technique integrates many significant empirically known properties of a fault and its radiation within a kinematic description of earthquake rupture as a propagating shear dislocation pulse. All significant steps of simulation are described, and key parameters needed to specify them are discussed. Examples are given that show how one can apply the described technique in practice.

In addition to the proposed integrated methodology, some particular approaches and algorithms should be mentioned as significant results, in particular:

1. The concept of conditioning the simulated fault motion through empirically defined far-field Fourier spectrum
2. The concept of mixing of deterministic and stochastic descriptions of the fault motion and a particular technique to combine these two descriptions
3. Incorporation of probabilistic distributions with controllable heavy upper tails for simulation of 2D field of final fault slip and of HF acceleration amplitudes, and the successful test of the lognormal law as applied to fault slip
4. A technique for modeling plausible spatial correlation structure of a broadband planar incoherent source

Acknowledgments

The research described herein would never been accomplished without the energetic and kind support of Giuliano Panza, who launched this study. Permanent support and advice of Viktor Pavlov are gratefully acknowledged. Discussions with Fabio Romanelli, Franco Vaccari, David Marsan, and Angela Sarao were valuable. The comments of M. Mai and an anonymous reviewer helped to improve the manuscript. The work was supported by the SAND group of the Abdus Salam International Center for Theoretical Physics, Trieste, Italy and by the Russian Foundation for Basic Research (grant 07-05-00775).

References

Aguirre, J., and Irikura, K. (2007), *Source characterization of mexican subduction earthquakes from acceleration source spectra for the prediction of strong ground motions*, Bull Seismol Soc Am, *97*, 1960–1969. doi:10.1785/0120050156

Aki, K. (1967), *Scaling law of seismic spectrum,* J Geophys Res, *72*, 1217–1231

Anderson, J. G., and Hough, S. E. (1984), *A model for the shape of the Fourier amplitude spectrum of acceleration at high frequencies,* Bull Seismol Soc Am,*74*, 1969–1993

Andrews, D. J. (1980), *A stochastic fault model, 1: Static Case,* J Geophys Res, *78*, 3867–3877

Andrews, D. J. (1981), *A stochastic fault model, 2: time-dependent case*, J Geophys Res, *86*, 10831–10834.

Atkinson, G. M. (1993), *Source spectra for earthquakes in eastern North America*, Bull Seismol Soc Am, *83*, 1778–1798

Bazzurro, P., Sjoberg, B., and Luco, N. (2004) *Post-elastic response of structures to synthetic ground motions*. Technical Report AT2, for PEER Lifelines Program project 1G00, AIR Worldwide Co., San Francisco

Beresnev, I. A. and Atkinson, G. M. (1999), *Generic finite-fault model for ground-motion prediction in Eastern North America,* Bull Seismol Soc Am, *89*, 608–625

Bernard, P., and Madariaga, R. (1984), *A new asymptotic method for the modeling of near-field accelerograms*, Bull Seism Soc Am, *74*, 539–557

Beroza G. C., and Mikumo, T. (1996), *Short slip duration in dynamic rupture in the presence of heterogeneous fault properties*, J Geophys Res, *101*, 22,449–22,460

Blandford, R. R. (1975), *A source theory for complex earthquakes*, Bull Seismol Soc Am, *65*, 1385–1405

Boatwright, J. (1982), *A dynamic model for far-field acceleration*, Bull Seism Soc Am, *72*, 1049–1068

Boatwright, J., Choy, G. L., and Seekins L. C. (2002), *Regional estimates of radiated seismic energy,* Bull Seismol Soc Am, *92*, 1241–1255

Boore, D. M. (1983), *Stochastic simulation of high-frequency ground motions based on seismological models of radiated spectra*, Bull Seism Soc Am, *73*, 1865–1894

Boore, D. M. (2003), *Simulation of ground motion using the stochastic method*, Pure appl Geophys, *160*, 635–676

Brune, J. N. (1970), *Tectonic stress and the spectra of seismic shear waves from earthquakes*, J Geophys Res, *75*, 4997–5009

Custodio, S., Liu, P. C., and Archuleta, R. J. (2005), *The 2004 Mw 6.0 Parkfield, California, earthquake: inversion of near-source ground motion using multiple data sets,* Geophys Res Lett, *32*(23)

Dalguer, L. A., Miyake, H., Day, S. M., and Irikura, K. (2008) *Surface rupturing and buried dynamic-rupture models calibrated with statistical observations of past earthquakes,* Bull Seismol Soc Am, *98*, 1147–1161

Dan, K., Watanabe, T., Sato, T., and Ishii, T. (2001), *Short-period source spectra inferred from variable-slip rupture models and modeling of earthquake fault for strong motion prediction*, J Struct Constr Eng AIJ, *545*, 51–62

Das, S., and Kostrov, B. V. (1983), *Breaking of a single asperity: rupture process and seismic radiation*, J Geophys Res, *88*, 4277–4288

Das, S., and Kostrov, B. V. (1988), *An investigation of the complexity of the earthquake source time function using dynamic faulting models*, J Geophys Res, *93*(B7), 8035–8050

Day, S. M., Gonzalez, S. H., Anooshehpoor, R., and Brune, J. N. (2008), *Scale-model and numerical simulations of near-fault seismic directivity*, Bull Seismol Soc Am, *98*, 1186–1206. doi: 10.1785/0120070190

Dreger, D., Nadeau, R. M., and Chung, A. (2007), *Repeating earthquake finite source models: strong asperities revealed on the San Andreas Fault*, Geophys Res Lett, *34*, L23302. doi: 10.1029/2007GL031353

Gusev, A. A. (1983), *Descriptive statistical model of earthquake source radiation and its application to an estimation of short-period strong motion*, Geophys J R Astr Soc, *74*, 787–808

Gusev, A. A. (1989), *Multiasperity fault model and the nature of short-period subsources*, Pure Appl Geophys, *130*, 635–660

Gusev, A. A. (1992) *On relations between asperity population and earthquake population on a fault.* Tectonophysics, *211*, 85–98

Gusev, A. A. (1996), *Peak factors of Mexican accelerograms: evidence of non-Gaussian amplitude distribution*, J Geophys Res, *101*, 20083–20090

Gusev A. (2010). *Approximate stochastic self-similarity of envelopes of high-frequency teleseismic P-waves from large earthquakes,* Pure Appl Geophys, in press.

Gusev, A. A., Guseva, E. M., and Panza, G. F. (2006), *Correlation between local slip rate and local high-frequency seismic radiation in an earthquake fault,* Pure Appl Geophys, *163*(7), 1305–1325. doi:10.1007/s00024-006-0068-4.

Gusev, A. A., Guseva, E. M., and Pavlov, V. M. (2009). *Modeling of the Ground Motion for the Petropavlovsk Earthquake of November 24, 1971* ($M = 7.6$), *Izvestiya*, Physics of the Solid Earth, *45*(5), 395–405 (Original Russian version: Fizika Zemli #5, 29–38, 2009)

Gusev, A. A., and Pavlov, V. M. (1991), *Deconvolution of squared velocity waveform as applied to study of non-coherent short-period radiator in earthquake source*, Pure Appl Geophys, *136,* 235–244

Gusev, A. A., and Pavlov, V. M. (2006), *Wideband simulation of earthquake ground motion by a spectrum-matching, multiple-pulse technique*, Intl Centre Theor Phys, Trieste, Preprint IC2006023, 27 pp. http://users.ictp.it/~pub_off/preprints-sources/2006/IC2006023P.pdf

Gusev, A. A., and Pavlov, V. M. (2009), *Broadband simulation of earthquake ground motion by a spectrum-matching, multiple-pulse technique*, Earthq Spectra, *25*, 257–276

Gusev, A. A., Pavlov, V., Romanelli, F., and Panza, G. (2008), *Low-frequency seismic ground motion at the pier positions of the planned Messina Straits Bridge for a realistic earthquake scenario*. In 2008 seismic engineering conference: commemorating the 1908 Messina and Reggio Calabria earthquake, Amer Inst Phys Conf Proc, *1020*(1), 362–369. doi:10.1063/1.2963858

Gusev, A., Radulian, M., Rizescu, M., and Panza, G. F. (2002) *Source scaling of intermediate-depth Vrancea earthquakes,* Geophys J Int, *151*, 879–889

Gusev, A. A., and Shumilina L. S. (2000), *Modeling the intensity-magnitude-distance relation based on the concept of an incoherent extended earthquake source*, Vulc Seis, *21*, 443–463 (English edition; original in Russian: (1999) 4–5, 29–40).

Halldorsson, B., and Papageorgiou A. S. (2005), *Calibration of the specific barrier model to earthquakes of different tectonic regions,* Bull Seism Soc Am, *95*, 1276–1300. doi:10.1785/0120040157

Hanks, T. C. (1979), *b values and* ω^{γ} *seismic source models: Implication for tectonic stress variations along active crustal fault zones and the estimation of high-frequency strong ground motion,* J Geophys Res, *84*, 2235–2242

Hanks, T. C., and William H. B. (2002), *A bilinear source-scaling model for M–log A observations of continental earthquakes*, Bull Seism Soc Am, *92*, 1841–1846

Hanks, T. C., and McGuire, R. K. (1981), *The character of high-frequency strong ground motion,* Bull Seism Soc Am, *71*, 2071–2095

Hartzell, S., Harmsen, S., Frankel, A., and Larsen, S. (1999), *Calculation of broadband time histories of ground motion: comparison of methods and validation using strong-ground motion from the 1994 Northridge earthquake,* Bull Seism Soc Am, *89*, 1484–1504

Hartzell, S., Guatteri, M., Mai, P. M., Liu, P. -Ch., and Fisk, M. (2005), Calculation of broadband time histories of ground motion, part II: kinematic and dynamic modeling using theoretical Green's functions and comparison with the 1994 Northridge earthquake, Bull Seismol Soc Am, 95614–95645. doi: 10.1785/0120040136

Heaton, T. H., (1990), *Evidence for and implications of self-healing pulses of slip in earthquake rupture,* Phys Earth Planet Inter, *64,* 1–20

Haskell, N. A. (1964). *Total energy and energy spectral density of elastic wave radiation from propagating faults,* Bull Seismol Soc Am, *54*, 1811–1841

Haskell, N. A., (1966), *Total energy and energy spectral density of elastic wave radiation from propagating faults. II. A stochastic fault model.* Bull Seism Soc Am, *56*, 125–140

Herrero, A., and Bernard, P. (1994), *A kinematic self-similar rupture process for earthquakes*, Bull Seism Soc Am, *84*, 1216–1228

Housner, G. W. (1955), *Properties of strong ground motion earthquakes*, Bull Seismol Soc Am, *45*, 197–218

Ide, S., and Takeo, M. (1997), *Determination of constitutive relations of fault-slip based on seismic wave analysis,* J Geophys Res, *102*, 27379–27391

Ide, S., and Aochi, H. (2005), *Earthquakes as multiscale dynamic ruptures with heterogeneous fracture surface energy*, J Geophys Res, *110*, B11303, doi:10.1029/2004JB003591

Irikura, K. (2007). *Predicting strong ground motions with a "Recipe",* Bull Earthq Res Inst Univ Tokyo, *81*, 341–352

Irikura, K., Kamae, K., *Estimation of strong ground motion in broad-frequency band based on a seismic source scaling model and an empirical Green's function technique*. Annali Di Geofisica, *37*, 6, pp 1721–1743 (1994)

Izutani, Y. (1984) *Source parameters relevant to heterogeneity of a fault plane*, J Phys Earth, *32*, 511–529

Joyner, W. B., (1984), *A scaling law for the spectra of large earthquakes,* Bull Seism Soc Am, *74*, 1167–1188

Kakehi, Y., and Irikura, K. (1996), *Estimation of high frequency wave radiation areas on the fault plane by the envelope inversion of acceleration seismograms*, Geophys J Int, *125*, 892–900

Kamae, K., and Irikura, K. (1998) Source model of the 1995 hyogo-ken nanbu earthquake and simulation of near-source ground motion, Bull Seism Soc Am, *88*, 400–412

Kanamori, H., and Allen, C. A., *Earthquake repeat time and average stress drop*, (Das, S., Boatwright, J., and Scholz, C. H., eds.,) Earthquake source mechanics, AGU, 227–235 (1986)

Kanamori, H., and Anderson, D. L. (1975), *Theoretical basis of some empirical relations in seismology*, Bull Seism Soc Am, *65*, 1073–1095

Kopnichev, Yu. F., and Shpilker, G. L. (1978) *Parameters of high-frequency radiation of earthquake source and the model of strong motion*. Doklady AN SSSR, 239, 193–196 (in Russian)

Kostrov, B. V. *Mechanics of the source of a tectonic earthquake*. (Nauka Moscow 1974) (in Russian).

Koyama, J. (1985). *Earthquake source time-function from coherent and incoherent rupture*, Tectonophysics 118, 227–242

Lavallee, D., and Archuleta, R. (2003). *Stochastic modeling of slip spatial complexities for the 1979 Imperial Valley, California, earthquake*, Geophys Res Lett, *30*, 1245. doi:10.1029/2002GL015839

Lavallee, D., Liu, P. -Ch., and Archuleta, R. J. (2006) *Stochastic model of heterogeneity in earthquake slip spatial distributions*, Geophys J Int, *165*, 622–640. doi: 10.1111/j.1365-246X.2006.02943.x

Lavallée, D., and Archuleta, R. J. (2005), *Coupling of the random properties of the source and the ground motion for the 1999 Chi Chi earthquake*, Geophys Res Lett, *32*, L08311. doi:10.1029/2004GL022202

Mai, P. M. (2004), Online database of finite-source rupture models, http://www.seismo.ethz.ch/srcmod

Mai, P. M., and Beroza, G. C. (2002), *A spatial random field model to characterize complexity in earthquake slip,* J Geophys Res, *107*, 2308. doi:10.1029/2001JB000588

Mai, P. M., Spudich, P., and Boatwright, J. (2005) *Hypocenter locations in finite-source rupture models,* Bull Seismol Soc Amer, *95,* 965–980. doi:10.1785/0120040111

Manighetti, I., Campillo, M., Sammis, C., Mai, P. M. and King, G. (2005), *Evidence for self-similar, triangular slip distributions on earthquakes: implications for earthquake and fault mechanics,* J Geophys Res, *110*, B05302. doi:10.1029/2004JB003174

Marsan, D., and Bean, C. (2003) Multifractal modelling and analyses of crustal heterogeneity. In Heterogeneity in the crust and upper Mantle (Goff, J. A., and Hollinger, K., eds) pp 207–236, (Kluwer Academic, New York)

Mendoza, C., and Hartzell, S. H. (1989), *Slip distribution of the 19 September 1985 Michoacan, Mexico, earthquake - near-source and teleseismic constraints*, Bull Seis Soc Am, *79*(3), 655–669

Morikawa, N., and Sasatani, T. (2004) *Source models of two large intraslab earthquakes from broadband strong ground motions*, BSSA, *94*(3), 803–817

Miyake, H., Iwata, T., and Irikura, K. (2003), *Source characterization for broadband ground-motion simulation: kinematic heterogeneous source model and strong motion generation area*, Bull Seism Soc Am, *93*, 2531–2545

Nagai, R., Kikuchi, M., and Yamanaka, Y. (2001), *Comparative study on the source processes of reccurent large earthquakes in Sanriku-oki Region: the 1968 Tokachi-oki earthquake and the 1994 Sanriku-oki Earthquake,* Zishin, J Seismol Soc Japan, *54*, 267–280

Nakahara, H. (2008) *Seismogram envelope inversion for high-frequency seismic energy radiation from moderate-to-large earthquakes*, Adv Geophys, *50*, 401–426

Nishimura, T., Nakahara, H., Sato, H., and Ohtake, M. (1996), *Source process of the 1994 far east off Sanriku earthquake, Japan, as inferred from a broad-band seismogram*, Sci Rep Tohoku Univ, *34*, 121–134

Oglesby D. D., Archuleta R. J. (1997) *A faulting model for the 1992 Petrolia earthquake: Can extreme ground acceleration be a sourse effect?* J Geophys Res, *102*(B6), 11.877–11.897

Ohno, S., Ohta, T., Ikeura, T., and Takemura, M. (1993) *Revision of attenuation formula considering the effect of fault size to evaluate strong-motion spectra in near field,* Tectonophysics, *218*, 69–81

Ordaz, M., and Singh, S. K. (1992), *Source spectra and spectral attenuation of seismic waves from Mexican earthquakes, and evidence of amplification in the hill zone of Mexico City,* Bull Seismol Soc Am, *82*, 24–43

Papageorgiou, A. S., and Aki, K. (1983), *A specific barrier model for the quantitative description of inhomogeneous faulting and the prediction of the strong ground motion, I: description of the model,* Bull Seismol Soc Am, *73*, 693–722

Papageorgiou, A. S., and Aki, K. (1985) *Scaling law of far-field spectra based on observed parameters of the specific barrier model*, Pure Appl Geophys, *123*, 354–374

Pavlov, V. M. (2002) *A convenient technique for calculating synthetic seismograms in a layered half-space,* Proceedings of the international conference on problems of geocosmos, St. Petersburg, 320–323

Pavlov, V. M. (2006), *Calculation of static displacements from force in a layered halfspace*, Volcanol Seismol, *4*, 25–33 (in Russian)

Pavlov, V. M. (2009), *Matrix impedance in the problem of calculation of synthetic seismograms in a uniformly layered isotropic elastic medium*, Fizika Zemli, *10*, 14–24 (in Russian, with parallel English edition)

Parvez, I. A., Gusev, A. A., Panza, G. F., and Petukhin, A. G. (2001), *Preliminary determination of the interdependence among strong-motion amplitude, earthquake magnitude and hypocentral distance for the Himalayan region*, Geophys J Int, *144*(3), 577–596

Petukhin, A. G., and Gusev, A. A. (2003), *The duration-distance relationship and average envelope shapes of small Kamchatka earthquakes*. Pure Appl Geophys, *160*, 1717–1743

Rautian, T. G., Khalturin V. I., and Dotsev, N. T. (1989). *Macroseismic magnitude* Voprosy Inzhenernoi Seismologii *30*, 98–109 (in Russian)

Sato, R. (1979) *Theoretical basis on relationships between focal parameters and magnitude*, J Phys Earth, *27*, 353–372

Schmitt, F., and Marsan, D. (2001) *Stochastic equations for continuous multiplicative cascades in turbulence*, Eur Phys J, *20*, 3–6

Scholz, C. (1982). *Scaling laws for large earthquakes and consequences for physical models*, Bull Seismol Soc Am *72*, 1–14

Scholz, C. H., Aviles C. A., and Wesnousky, S. G. (1986) *Scaling Differences Between Large Interplate and Intraplate Earthquakes*, Bull Seismol Soc Amer *76*, 65–70, February

Sekiguchi, H., Irikura, K., Iwata, T., Kakehi, Y., and Hoshiba, M. (1996), *Minute locating of faulting beneath Kobe and the waveform inversion of the source process during the 1995 Hyogo-ken Nanbu, Japan, earthquake using strong ground motion records*, J Phys Earth, *44*(5), 473–487

Sekiguchi, H., and Iwata, T. (2002), *Rupture process of the 1999 Kocaeli, Turkey, earthquake estimated from strong-motion waveforms,* Bull Seis Soc Am *92*(1), 300–311

Silberschmidt, V. V. (2000) *Dynamics and scaling characteristics of shear crack propagation,* Pure Appl Geophys, *157,* 523–538

Singh, S. K., Ordaz, M., Anderson, J. G., Rodriguez, M., Quaas, R., Mena, E., Ottaviani, M., and Almora, D. (1989) *Analysis of near source strong-motion recordings along the Mexican subduction zone,* Bull Seism Soc Am, 79, 1697–1717

Somerville, P., K. Irikura, R. Graves, S. Sawada, D. Wald, N. Abrahamson, Y. Iwasaki, T. Kagawa, N. Smith, and A. Kowada (1999). *Characterizing crustal earthquake slip models for the prediction of strong motion,* Seism Res Lett 70, 59–80

Spudich, P. and L. N. Frazer. (1984), *Use of ray theory to calculate high-frequency radiation from earthquake sources having spatially variable rupture velocity and stress drop,* Bull Seism Soc Am, *74*, 2061–2082

Thatcher, W., and Hanks, T. C. (1973), *Source parameters of Southern California earthquakes*, J Geophys Res, *78*, 8547–8576

Trifunac, M. D., and Lee V. W. (1989), *Preliminary empirical model for scaling Fourier amplitude spectra of strong ground acceleration in terms of earthquake magnitude, source to station distance and recording site conditions*, Earthq Eng Struct Mech, *18*, 999–1016

Tsai, C. -C. P. (1997a), *Ground motion modeling for seismic hazard analysis in the near-source regime: an asperity model*, Pure Appl Geophys, *149*, 265–297 (0033-4553:97:020265-33)

Tsai, C. -C. P. (1997b), *Slip, stress drop and ground motion of earthquakes: a view from the perspective of fractional Brownian motion.* Pure Appl Geophys, 149, 689–706

Valensise, L., and Pantosti, D. (1992), *A 125 kyr-long geological record of seismic source repeatability: the Messina Straits (Southern Italy) and the 1908 earthquake (Ms = 7.5),* Terra Nova, *4*, 472–483

Wells, D. L., and Coppersmith, K. J. (1994), *New empirical relationships among magnitude, rupture length, rupture width, rupture area, and surface displacement*, Bull Seism Soc Am, *84*(4), 974–1002

Yagi, Y. (2004), *Source rupture process of the 2003 Tokachi-oki earthquake determined by joint inversion of teleseismic body wave and strong ground motion data*. Earth Planets Space, *56*(3), 311–316

Yin, Z. -M., and Ranalli, G. (1995) *Modeling of earthquake rupturing as a stochastic-process and estimation of its distribution function from earthquake observations*. Geophys J Int, *123*, 838–848

Yu, G., Khattri, K. N., Anderson, J. G., Brune, J. N., and Zeng, Y. (1995), *Strong ground motion from the Uttarkashi, Himalaya, India, Earthquake: comparison of observations with synthetics using the composite source model,* Bull Seism Soc Am, *85*, 31–50

Zeng, Y., Anderson, J. G., and Yu, G. (1994) *A composite source model for computing realistic synthetic strong ground motions*, Geophys Res Lett, *21*, 725–728

Zeng, Y., Anderson J. G., and Su, F. (1995), *Subevent rake and scattering effects in realistic strong ground motion simulation,* Geophys Res Lett, *22*, 17–20

Zollo, A., Bobbio, A., Emolo, A., Herrero, A., and De Natale, G. (1997), *Modelling of ground acceleration in the near source range: the case of 1976, Friuli earthquake (M = 6.5), northern Italy*, J Seismol 1:305–319

(Received April 8, 2009, revised March 23, 2010, accepted April 8, 2010, Published online June 1, 2010)